Homoclinic Orbits and Solitary Waves in a One-Dimensional Array of Chua's Circuits

Vladimir I. Nekorkin, Victor B. Kazantsev, Nikolai F. Rulkov,
Manuel G. Velarde, and Leon O. Chua, *Fellow, IEEE*

***Abstract*— The possible propagation of solitary waves in a one-dimensional array of inductively coupled Chua's circuits is considered. We show that in the long-wave limit, the problem can be reduced to the analysis of the homoclinic orbits of a dynamical system described by three coupled nonlinear ordinary differential equations modeling the individual dynamics of a single Chua's circuit. Analytical, numerical, and experimental results concerning the bifurcations associated with the appearance of homoclinic orbits and thus with the propagation of solitary waves are provided.**

I. Introduction

MODELS composed of coupled nonlinear oscillators play a significant role in the understanding of the dynamical behavior of many systems which are studied in nonlinear physics, biology, chemical kinetics and in other branches of science. Many of these systems can be described as a group of identical or almost identical interacting self-excited oscillators which are located at the junctions of a space lattice or cellular neural network. In particular this sort of system has been considered in the studies of Josephson arrays [1], arrays of reaction cells [2], collective behavior of biological oscillators [3], neural networks [4], nonlinear synchronization arrays [5], and arrays of electronic oscillators [6]–[8]. Some regimes of collective behavior of these systems can be considered from the viewpoint of spatio-temporal dynamics of a nonequilibrium medium. Therefore, the analysis of these regimes can be based on methods which have been developed for the studies of nonlinear waves and structures in continuously distributed systems (see e.g., [9]–[11]).

Recent interest in the studies of spatio-temporal dynamics of coupled electronic oscillators is connected with the use of electronic circuits for modeling collective behavior of biological systems. In a number of papers [12]–[14] arrays of *resistively* coupled Chua's circuit's have been employed as models of self-excited media. It has been shown that these arrays can sustain wave front propagation and generate spiral waves [15].

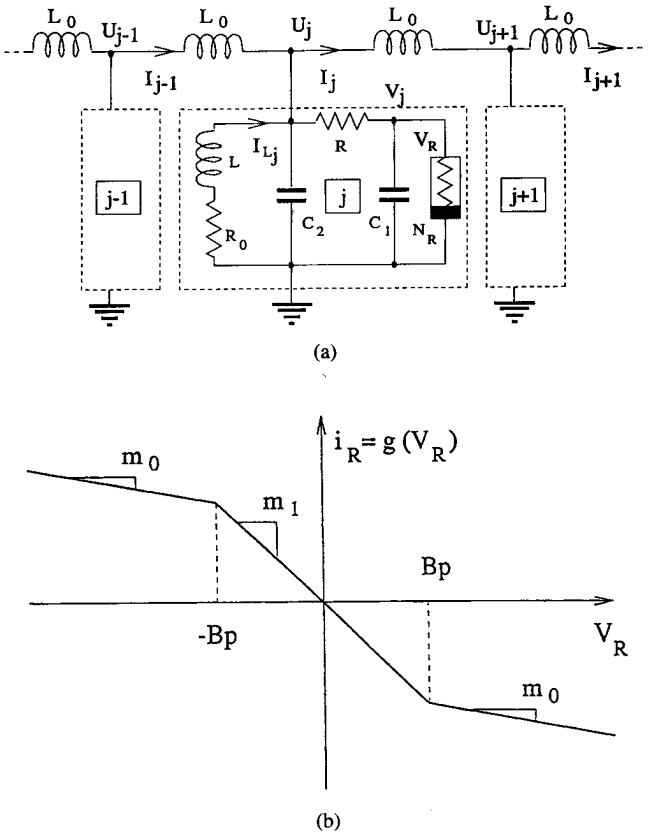

Fig. 1. (a) Block diagram of the 1-D array of Chua's circuits coupled by the inductors/self L_0. (b) Three-segment piecewise-linear $v - i$ characteristic of the nonlinear resistor N_R.

In this paper we study the existence of solitary waves in 1-D array of *inductively* coupled Chua's circuits. In the remainder of this section we show how the problem of the existence of the solitary waves can be reduced to analyzing the bifurcations of homoclinic orbits in an auxiliary system which actually describes the behavior of an individual circuit. In Section II we provide the results obtained about the homoclinic orbits associated with solitary wave solutions of the array. In Section III we consider conditions for solitary wave propagation. Appendices A–D contain some results of the qualitative analysis of the dynamical system associated with the array.

The 1-D array of inductively coupled Chua's circuits (see diagram in Fig.1(a)) can be described by the following set of

Manuscript received November 4, 1994; revised January 15, 1995. This research has been supported by DGICYT (Spain) under Grant PB 93-81, by the European Union under Grant ERBCHRXCT 93-107 and by the U.S. Office of Naval Research under Grant N00014-89-J-1402. This paper was recommended by Guest Editor L. O. Chua.

V. I. Nekorkin and V. B. Kazantsev are with the Radiophysical Department, Nizhny-Novgorod State University, 603600 Nizhny-Novgorod, Russia.

N. F. Rulkov is with the Institute for Nonlinear Science, University of California, San Diego, La Jolla, CA 92093 USA.

M. G. Velarde is with the Instituto Pluridisciplinar, Universidad Complutense, Madrid 28 040, Spain.

L. O. Chua is with the Department of Electrical Engineering and Computer Sciences, University of California, Berkeley, CA 94720 USA.

IEEE Log Number 9414154.

equations:

$$\begin{cases} C_1\frac{dV_j}{dt} &= -g(V_j) + G(U_j - V_j), \\ C_2\frac{dU_j}{dt} &= G(V_j - U_j) + I_{L_j} + I_{j-1} - I_j, \\ L\frac{dI_{L_j}}{dt} &= -U_j - R_0 I_{L_j}, \\ L_0\frac{dI_j}{dt} &= U_j - U_{j+1} \end{cases} \tag{1}$$

$$I_0 = I_1,\ U_{N+1} = U_N$$

$$j = 1, 2, \ldots, N$$

where V_j, U_j, and I_{L_j} are the voltage across the capacitor C_1, the voltage across the capacitor C_2, and the current through the inductor L, respectively. I_j is the current through the coupling inductor L_0. The function g(V) is the voltage–current characteristic of the nonlinear resistor shown in Fig. 1(b). The index j stands for the variables of the j th cell of the array. N is the number of cells in the array. In dimensionless form equations (1) become

$$\begin{cases} \frac{dx_j}{d\tau} &= \alpha(y_j - x_j - f(x_j)), \\ \frac{dy_j}{d\tau} &= x_j - y_j + z_j + w_{j-1} - w_j, \\ \frac{dz_j}{d\tau} &= -\beta y_j - \gamma z_j, \\ \frac{dw_j}{d\tau} &= d(y_j - y_{j+1}) \end{cases} \tag{2}$$

$$j = 1, 2, \ldots, N$$

where

$$\tau = \frac{G}{C_2}t,\ x_j = \frac{V_j}{B_p},\ y_j = \frac{U_j}{B_p},\ z_j = \frac{I_{L_j}}{B_p G},\ w_j = \frac{I_j}{B_p G}$$

and

$$\alpha = \frac{C_2}{C_1},\ \beta = \frac{C_2}{LG^2},\ \gamma = \frac{R_0 C_2}{LG},\ d = \frac{C_2}{L_0 G^2}.$$

Note that α, β, γ characterize the individual dynamics of the cell in the array, and have positive values. The parameter d characterizes the strength of the coupling between the elements. The nonlinear function $f(x)$ describes the three-segment piecewise-linear resistor characteristic $g(V)$, i.e.,

$$f(x) = \begin{cases} bx + a - b & \text{if } x \geq 1 \\ ax & \text{if } -1 \leq x \leq 1 \\ bx - a + b & \text{if } x \leq -1 \end{cases} \tag{3}$$

with $a = \frac{m_1}{G}$, $b = \frac{m_0}{G}$.

A "travelling" wave solution of the system described by (2) and (3) is

$$\begin{aligned} x_j(t) &= x(\xi) \\ y_j(t) &= y(\xi) \\ z_j(t) &= z(\xi) \\ w_j(t) &= w(\xi) \end{aligned} \tag{4}$$

where $\xi = t - jh$, $0 < h$ is a parameter. Substituting (4) into (2) we obtain

$$\begin{cases} \dot{x} &= \alpha(y - x - f(x)), \\ \dot{y} &= x - y + z + w(\xi - h) - w(\xi), \\ \dot{z} &= -\beta y - \gamma z, \\ \dot{w} &= d(y(\xi) - y(\xi + h)) \end{cases} \tag{5}$$

where the dot denotes differentiation with respect to ξ. Notice that ξ is the coordinate moving along the array with a velocity equal to $c = 1/h$. Let us assume that h is sufficiently small (i. e., c is sufficiently large). Then the two difference terms in equation (5) can be replaced approximately by the first derivatives $\dot{w}$ and $-\dot{y}$ (with respect ξ), respectively, and we obtain the following system of coupled first-order *ordinary* differential equations

$$\begin{cases} \mu\dot{x} &= y - x - f(x)), \\ \dot{y} &= \frac{1}{\delta}[x - y + z], \\ \dot{z} &= -\beta y - \gamma z \end{cases} \tag{6}$$

where $\mu = \frac{1}{\alpha}$, $\delta = 1 - \frac{d}{c^2}$. This system describes the waveforms of the travelling waves which can propagate with velocity c along the array.

Solitary waves of the model (2) correspond to nonconstant solutions of (6) which satisfy the condition

$$\lim_{|\xi| \to \infty} (x(\xi), y(\xi), z(\xi)) = 0. \tag{7}$$

Condition (7) is satisfied by the homoclinic orbits of the system (6).

Observe that in the case of $\delta = 1$ the system (6) coincides with the equations describing the local cell of the array.[1] Therefore, the following investigation is important not only from the point of view of the travelling wave model (2), but also from the viewpoint of canonical Chua's Circuit dynamics [17], [18].

II. Homoclinic Orbits

In this section we investigate the homoclinic bifurcations of the system (6) which indicates the existence of solitary waves in the array (1). Using analytical and numerical analyses we evaluate the parameter values for the appearance of homoclinic orbits in the phase space of the system (6). This section is divided into three subsections. Each subsection deals with a different approach to the investigation of the homoclinicity. In Section II–A the existence of homoclinic orbits is proved by a qualitative analysis of the trajectory behavior in the phase space of the dynamical system (6). In Section II–B these results are exemplified by numerical simulations of the system (6). Finally in Section II–C we show the results of our experimental studies dealing directly with real electronic circuits modeling the system (6).

[1] This is a typical situation for inductive coupling (see [16]).

A. Homoclinic Orbits. Phase space Analysis

Consider the behavior of the trajectories in the phase space of the system (6) as a function of the parameters of the system. Let us restrict our considerations to the parameter range:

$$\begin{array}{llll} \mu \ll 1, & d > 0, & \delta > 0, & \beta > \beta_{ab}, \\ \gamma \geq 0, & a < -1, & -1 < b < 0 & \end{array} \tag{8}$$

with

$$\beta_{ab} \equiv max\{\beta_a, \beta_b\}$$

$$\beta_q \equiv \frac{\delta}{4}\left[\gamma - \frac{q}{\delta(q+1)}\right]^2 + \frac{1}{4}\left[\frac{\gamma^2}{(q+1)^2} - \frac{q^2}{\delta^2(q+1)^4}\right]\mu + O(\mu^2)$$

where the index q can take one of two values, a or b. When (8) is satisfied, the system (6) has three stationary points:

$$O(0,0,0)\ ,\ P^+(x_0, y_0, z_0)\ ,\ P^-(-x_0, -y_0, -z_0).$$

The coordinates of these stationary points are given in terms of the parameters of the system as follows:

$$x_0 \equiv \frac{(\gamma+\beta)D}{\beta - \gamma B}, \quad y_0 \equiv \frac{\gamma D}{\beta - \gamma B}, \quad z_0 \equiv -\frac{\beta D}{\beta - \gamma B}, \qquad D \equiv \frac{b-a}{b+1}, \quad B \equiv -\frac{b}{(b+1)}. \tag{9}$$

Each of these stationary points have a pair of complex-conjugate eigenvalues. The stationary point O is a saddle-focus (see Appendix A) with a one-dimensional unstable manifold $W^u_\mu(O)$ and a two-dimensional stable manifold $W^s_\mu(O)$. The manifold $W^u_\mu(O)$ consists of the point O and two outgoing trajectories W^u_1 and W^u_2. In the (x, y, z)-phase space, the trajectory W^u_1 goes into the region $x > 0$, and the trajectory W^u_2 into the region $x < 0$. The stationary points $P^\pm$ may be either stable foci (in the parameter region G_s, see Fig. 2) or saddle-foci (in the parameter region G_u, Fig. 2) with one-dimensional stable manifolds $W^s_\mu(P^\pm)$ and two-dimensional unstable manifolds $W^u_\mu(P^\pm)$. The points $P^\pm$ change stability at the bifurcation values $\beta = \beta_s$where

$$\beta_s \equiv -\frac{[1 + \frac{\delta(b+1)}{\mu}][\gamma^2 + \gamma(\frac{1}{\delta} + \frac{b+1}{\mu}) + \frac{b}{\mu\delta}]}{\gamma + \frac{1}{\delta}}. \tag{10}$$

At the bifurcation values the trajectories located on the manifolds $W^u_\mu(P^\pm)$ are equivalent to the trajectories of elliptic points in a two-dimensional manifold.

Let us consider the homoclinic orbits in the phase space of system (6) with the parameters taken in the region G_u (see Fig. 2). Let us examine the homoclinic orbits formed by the trajectory W^u_1. Since the vector field of the system (6) is invariant under the transformation

$$(x, y, z) \rightarrow (-x, -y, -z) \tag{11}$$

the homoclinic orbit formed by W^u_1 coexists with the homoclinic orbit formed by W^u_2.

Consider now the behavior of the trajectory W^u_1 when in the system (6) one has $\mu \ll 1$ which is the coefficient associated with the highest derivative of the system. In this case we have

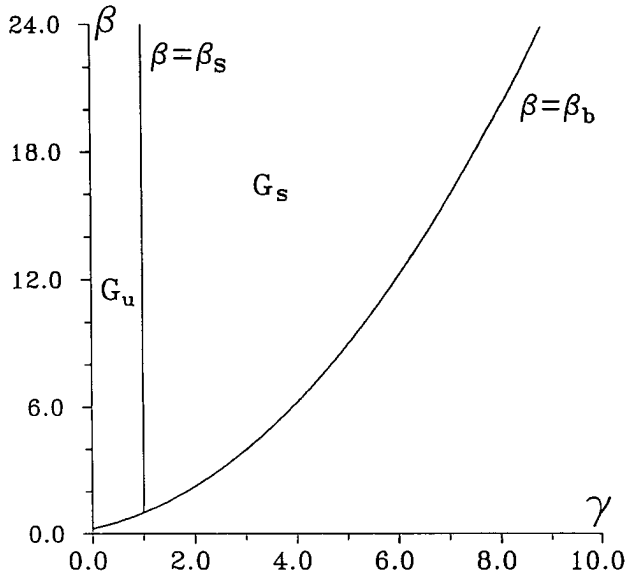

Fig. 2. Two-dimensional parametric planar representation (γ, β) with $a = -2$, $b = -1/2$, $\mu = 0.01$,, and $\delta = 0.95$. For the parameter values in the region G_s, the stationary point P^+ is a stable focus. In the region G_u the point P^+ is a saddle-focus.

a singular perturbation multiscaling problem, and the motion in the three-dimensional phase space has both fast and slow features [19].

We start our analysis with $\mu = 0$. In this case a two-dimensional manifold W_0 of slow motions exists in the (x, y, z)-phase space of the system (6). The shape of the manifold is given by

$$W_0 : \{(x, y, z) \mid y = x + f(x)\}. \tag{12}$$

Comparing (12), (35), and (36) (see Appendix A) we note that W_0 coincides with the two-dimensional manifold of the stationary points O and P^+. In the regions $x \geq 1$, $x \leq -1$, the manifold W_0 is given by the planes $W^u_0(P^\pm)$. In the region $\mid x \mid \leq 1$, W_0 is the plane $W^s_0(O)$ (see Fig. 3). Therefore, the character of the slow motion on the manifold W_0 is conditioned by the complex-conjugate eigenvalues of the points $P^\pm$ and O. As shown in Appendix C, the trajectories located on the planes $W^u_0(P^\pm)$ form unstable foci, and the trajectories on the plane $W^s_0(O)$ form a stable focus. Outside the surface W_0 the dynamics of the system generates fast motions with

$$z = const., \quad y = const. \tag{13}$$

It can be shown (see equation (6)) that the planes $W^u_0(P^\pm)$ attract, and the plane $W^s_0(O)$ ejects the trajectories going to the regions of fast motions. The qualitative behavior of the trajectories corresponding to fast and slow motions is shown in Fig. 3.

Now consider $0 < \mu \ll 1$. In this case the manifold of slow motions W_μ of the system (6) consists of two-dimensional manifolds of the stationary points O and $P^\pm$. Within the region $x \geq 1$ the manifold W_μ is formed by the plane $W^u_\mu(P^+)$, and

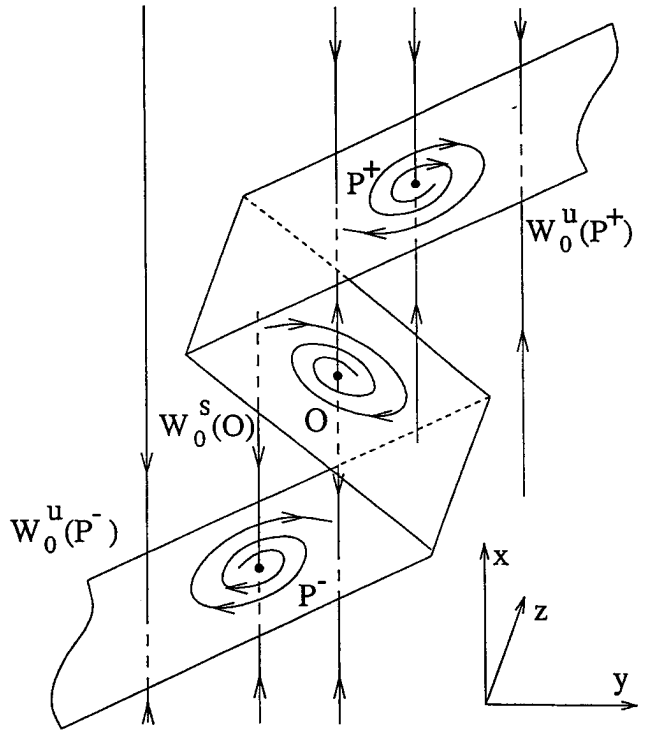

Fig. 3. Qualitative picture of the phase portrait of the system (6) in the relaxation regime with $\mu = 0$.

in the region $\mid x \mid \leq 1$ it is formed by the plane $W^s_\mu(O)$ (see Appendix A, formulas (29) and (35) for detail). The shape of W_μ is presented in Fig. 4(a). It is shown in Appendix B that $W^s_\mu(O)$ and $W^u_\mu(P^+)$ intersect the plane

$$U_{+1} : \{(x, y, z) \mid x = 1\} \tag{14}$$

at the lines l^s_μ and l^u_μ, respectively, and the lines l^s_μ and l^u_μ intersect each other at the point $L(y_l, z_l)$ (see Fig. 4(b), formulae (40)).

Since the point L lies at the intersection between $W^u_\mu(P^+)$ and $W^s_\mu(O)$, there is a trajectory that originates from the stationary point P^+, passes through L, and then tends to the stationary point O. In Fig. 4(a) this trajectory is shown by solid line and marked by Γ_l. The trajectory Γ_l forms a heteroclinic orbit.

Besides L, the lines l^s_μ and l^u_μ contain the points K and M which are essential for understanding the dynamics of the system. The location of these points is shown in Fig. 4(b), and their coordinates are determined in Appendix C, formulae (41) and (42). These points divide the trajectories located in the planes $W^u_\mu(P^+)$ and $W^s_\mu(O)$ into trajectories which leave the planes and trajectories which come to the planes at the lines l^s_μ and l^u_μ. The trajectories passing above the point M come to the plane $W^s_\mu(O)$. The trajectories passing below the point K come to $W^u_\mu(P^+)$.

Since $0 < \mu \ll 1$, the slow motions take place not only on the planes $W^s_\mu(O)$ and $W^u_\mu(P^+)$, but also in some *thin layers* (thicknesses of order of μ) containing these planes. Let us consider the trajectory W^u_1 which originates from the stationary point O and describes its evolution in the (x, y, z) phase space. This trajectory has intervals of fast and slow

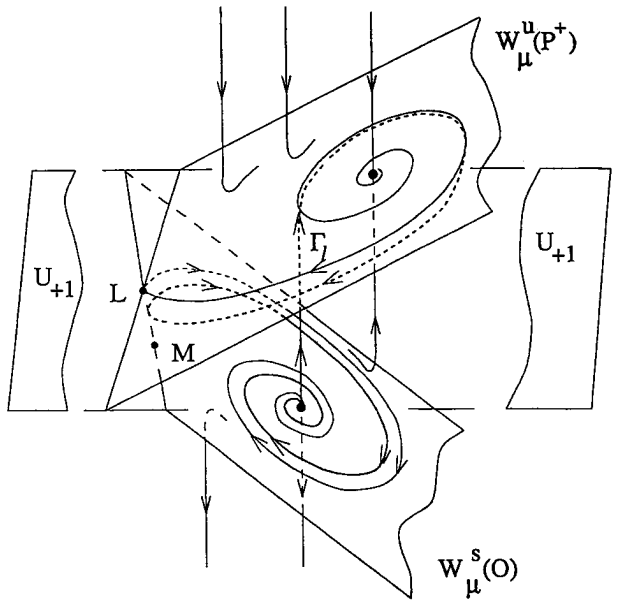

(a)

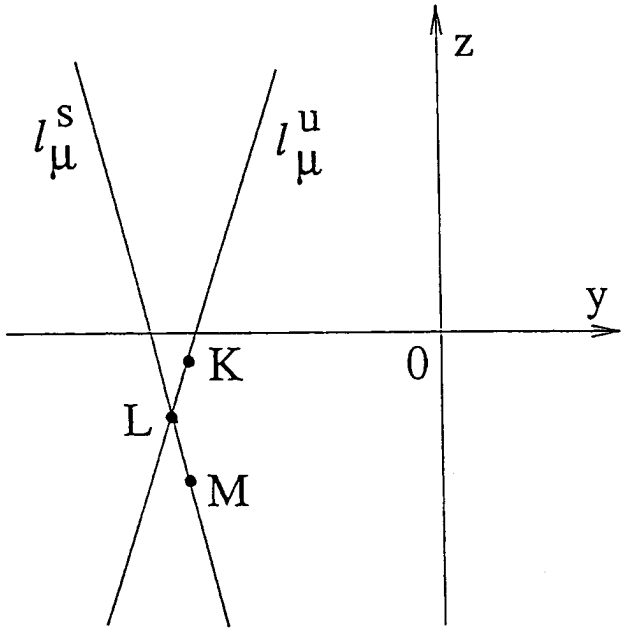

(b)

Fig. 4. (a) A portion of the qualitative picture of the phase portrait of the system (6) in the relaxation regime with $0 < \mu \ll 1$. (b) Relative location of cross sections of the manifolds $W^u_\mu(P^+)$ and $W^s_\mu(O)$ at the plane $x = 1$.

motions. Fast motion along the trajectory occurs in the region of the phase space which is located outside the thin layers associated with the planes $W^s_\mu(O)$ and $W^u_\mu(P^+)$ (see Fig. 4(a)). In this region of the phase space the shape of the trajectory W^u_1 is close to the straight line $\{z = 0, y = 0\}$. After passing this region the trajectory W^u_1 comes into the thin layer of slow motions associated with the plane $W^s_\mu(P^\pm)$. In this layer the behavior of the trajectory is qualitatively similar to the behavior of the nearest trajectory located in the plane $W^s_\mu(P^\pm)$. Since under the conditions (8) the trajectories in the plane $W^s_\mu(P^\pm)$ have the shape of an unwinding spiral,

the trajectory W_1^u will also have an interval of the form of an unwinding spiral (see Fig. 4(a)). Therefore, being in the thin layer of slow motions the trajectory W_1^u makes one or several rotations under the plane $W_\mu^u(P^+)$ and then intersects the plane U_{+1}. Let M_1^u be the point of the first intersection of the trajectory W_1^u with the plane U_{+1} when it leaves from the domain $x > 1$. Two statements concerning the location of the point M_1^u can be made based on the fact that the trajectory W_1^u passes the region of slow motion under the plane $W_\mu^u(P^+)$.

- M_1^u is located to the right of the line l_μ^u.
- The point M_1^u is located in a μ-neighborhood of the line l_μ^u.

Now let us consider the line l_μ^s which is given by the intersection between the planes $W_\mu^s(O)$ and U_{+1} (see Fig. 4(b) and Appendix B). In the plane U_{+1} this line divides the right μ-neighborhood of the line l_μ^u into two domains U_μ^s and U_μ^u located to the right and to the left of the line l_μ^u, respectively. The point M_1^u can belong to either one of these domains or to the line l_μ^s. If the point M_1^u is in the domain U_μ^s then after intersecting the plane U_{+1} the trajectory W_1^u goes into the region of fast motions *under the plane* $W_\mu^s(O)$. If the point M_1^u is in the domain U_μ^u then after intersecting the plane U_{+1} the trajectory W_1^u stays in the layer of slow motions in a μ-neighborhood of $W_\mu^u(P^+)$, and therefore, *above the plane* $W_\mu^s(O)$. Finally, if $M_1^u \in l_\mu^s$, then the trajectory W_1^u belongs to the plane $W_\mu^s(O)$ and with $\xi \to +\infty$ tends to the stationary point O. Since W_1^u originates at O, the last case corresponds to the existence of a homoclinic orbit in the phase space of the system (6).

Similar arguments can be used for the analysis of homoclinic bifurcations in the parameter region G_s. The main difference from the case considered above is that in the region G_s one can only find the bifurcations of the homoclinic orbit which make only one rotation in the slow motions layer. The detailed description of the bifurcations of this type is presented in Section II–C.

In order to obtain the parameter values corresponding to a homoclinicity we use the property of piecewise-linearity of the function (3)[2]. First, we find the point M_0^u where the trajectory W_1^u intersects the plane U_{+1} for the first time. It follows from (34) that the coordinates of this point are

$$x = 1\,, \quad y = y_0^u\,, \quad z = z_0^u \tag{15}$$

$$y_0^u \equiv -\frac{1}{k_4^a}\,, \; z_0^u \equiv -\frac{1 + k_4^a - k_3^a}{k_4^a}$$

where k_3^a and k_4^a are given by (32). In the region $x > 1$, the solution of the system (6) corresponding to the trajectory passing through the point M_0^u can be presented in the form

$$x = \varphi_1(\xi, C_u)\,, \quad y = \varphi_2(\xi, C_u)\,, \quad z = \varphi_3(\xi, C_u)\,. \tag{16}$$

Since the system (6), for region $x > 1$, is linear, the functions φ may be easily obtained. The equation

$$\varphi_1(\xi, C_u) = 1 \tag{17}$$

enables us to determine the interval of "time" $\xi = \tau$ required for the trajectory to reach the point M_1^u starting at M_0^u. The existence of the point M_1^u is guaranteed when the parameter values are taken in the region G_u. Therefore, the solution of equation (17) exists for the considered parameter values. The coordinates of the point M_1^u can be given in the form

$$x = 1\,, \quad y = y_1^u\,, \quad z = z_1^u \tag{18}$$

with

$$y_1^u \equiv \varphi_2(\tau, C_u)\,, \; z_1^u \equiv \varphi_3(\tau, C_u).$$

It follows from (18) and (37) (see Appendix B) that the point $M_1^u \in l_\mu^s$ if the parameters of the system (6) satisfy the equation

$$k_1^a \varphi_2(\tau, C_u) + k_2^a \varphi_3(\tau, C_u) + 1 = 0. \tag{19}$$

Equation (19) defines the bifurcation set Π corresponding to the appearance of the single-loop homoclinic orbit[3] of the system (6) associated with the stationary point O. Note that a single-loop orbit can have a rather complicated shape because such orbits may rotate many times in a thin layer near the plane $W_\mu^u(P^+)$. Unfortunately, the equation (17) can not be solved exactly by analytical methods. However, it can be solved numerically. The results of our numerical analysis of the bifurcation set Π using the equation (17) will be discussed in Section II–B. The bifurcation set Π can also be examined using an approximate description of the behavior of the trajectory W_1^u when it can be divided into fast and slow motions. Then the fast and slow motions can be considered separately. The fast part of the motion of W_1^u is close to the line $\{y = z = 0\}$.

Let us consider in detail the slow part of the motion of the trajectory W_1^u. It has been determined above that if the homoclinic orbit exists, then the point $M_1^u \in l_\mu^s$ is located between the points L and M. First, we discuss how the trajectory W_1^u approaches the point M_1^u. As it follows from (37) (see Appendix B), when $0 < \mu \ll 1$, the line l_μ is close to the line $y = a+1$. Therefore, when the trajectory W_1^u comes close to the point M_1^u, its motion satisfies the condition $\dot{y} \approx 0$. On the other hand, in order to remain in the thin layer of slow motions the trajectory W_1^u must satisfy the condition $\dot{x} \approx 0$ in the vicinity of the point M_1^u. Taking into account these two facts we find that the point M_1^u with such properties in the plane U_{+1} is located in the vicinity of the point

$$y = y_a\,, \; z = z_a$$

where

$$y_a \equiv a + 1\,, \; z_a \equiv a.$$

Besides, in the layer of slow motions W_1^u moves very close to the plane $W_\mu^u(P^+)$. Therefore, during the slow motion W_1^u may be approximated by some trajectory located in the plane $W_\mu^u(P^+)$. Taking into account the properties of the trajectory W_1^u near the point M_1^u we choose the trajectory from the plane $W_\mu^u(P^+)$ which passes through the point

$$y = y_a\,, \; z = z_a.$$

[2]Notice that the formulae obtained using this approach are correct for any value of μ

[3]Multiloop homoclinic orbits will be discussed later.

Let Γ_a denote the chosen trajectory from the plane $W^u_\mu(P^+)$. From (37) (see Appendix B) it follows that in the (x, y, z)-phase space the trajectory Γ_a passes through the point $A(x_a, y_a, z_a)$,where

$$x_a \equiv 1 - \frac{[a\gamma + \beta(a+1)]}{\delta(b+1)^3}\mu^2 + O(\mu^3).$$

In order to prove that the point A is close to the line l^s_μ we evaluate the distance between them. From (37) (see Appendix B) follows that the distance R between A and l^s_μ is

$$R = \frac{|\gamma a + \beta(a+1)|}{\delta}\sqrt{\frac{1}{(a+1)^4} + \frac{1}{(b+1)^6}}\,\mu^2 + O(\mu^3)$$

which is of order μ^2, i.e., it is a small quantity. Hence, the set of parameter values, Π_{approx}, approximating the bifurcation set Π may be obtained by analyzing the conditions which are applied to the trajectory Γ_a to be the best approximation of the trajectory W^u_1. These conditions may be considered as the boundary problem for the two-dimensional system (42) (see Appendix C). The solution of the boundary problem give us the set of the parameter values Π_{approx}. This solution takes the form of the following equation:

$$\frac{D_\mu\sqrt{\beta I_\mu}}{\sqrt{\delta(\beta I_\mu - \gamma B_\mu)}} = -\left(a + 1 - \frac{\gamma D_\mu}{\beta I_\mu - \gamma B_\mu}\right) \exp\left\{\frac{h}{\omega}\left(2\pi n - \arctan\frac{2\omega}{\gamma + \frac{B_\mu}{\delta}}\right)\right\} \qquad (20)$$

$$n = 1, 2, \ldots$$

where $B_\mu, I_\mu, D_\mu, \omega$ and h are given by (42) and (43) (see Appendix C). The index n characterizes the number of rotations made by the trajectory W^u_1 while it unwinded around the stationary point P^+ moving in the layer of slow motions. The solutions of the equation (20) obtained for $n = 1, 2, 3$ and 4 with the fixed parameter values $a = -2$, $b = -1/2$, $\mu = 0.01$ are shown in Fig. 5 by dashed curves in the parameter plane (β, γ).

We would like to emphasize that all curves defined by (20) start from the same point Π_0 of the plane (β, γ). The point Π_0 has the coordinates

$$\gamma = \frac{B_\mu}{\delta},\ \beta = \frac{[D_\mu + (a+1)B_\mu]^2}{\delta(a+1)^2}. \qquad (21)$$

The behavior of these curves near the point Π_0 has the following explanation. At the parameter point Π_0 the system (42) is conservative and, therefore, the trajectories on the plane $W^u_\mu(P^+)$ given by this system are equivalent to the trajectories near an elliptic point. In this case the trajectory Γ_a is closed and have the form of an ellipse. The point A is the leftmost point of the ellipse. The ellipse is "nearly" tangential[4] to the line l^s_μ. Therefore, we use the contour Γ_0 as an interval of trajectories which approximate a homoclinic orbit. The contour Γ_0 goes along the ellipse which is tangential to the line l^s_μ and intersect the line $\{y = 0,\ z = 0\}$ originating from the stationary point O, simultaneously. It is clear that the contour Γ_0 can approximate a homoclinic orbit making any number of rotations n in a neighborhood of the stationary points P^+.

[4]Tangency occurs at the "zeroth-" order of the approximation with respect to the small parameter μ

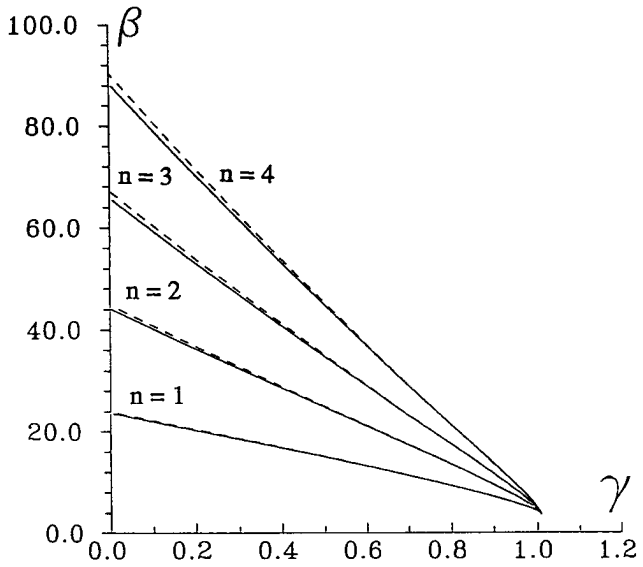

Fig. 5. Bifurcation curves of the homoclinicity of the system (6) plotted in the parameter plane (γ, β) with $a = -2$, $b = -1/2$, $\mu = 0.01$, $\delta = 0.95$. The results of numerical simulation are shown with solid lines. Dashed lines are plotted using the approximate formula (20).

B. Homoclinic Orbits. Numerical Simulations

In numerical simulations the bifurcation set Π can be analyzed in two ways. The first way is based on the results of Section II–A. It consists of a numerical solution of (17) together with (19) to calculate the parameter values of the bifurcation set. The second way consists of a numerical integration of the system (6) in the region $x \geq 1$ with initial conditions at the point M^u_0. The integration is stopped at the point M^u_1, which is the first intersection of the trajectory with the plane U_{+1}. Locating the point M^u_1 for different parameter values, we find the set of the parameter values which satisfy the condition $M^u_1 \in l^s_\mu$ (see, Section II–A). In our numerical analysis we used both methods. We have found that both methods give the results which are very close to each other.

In this section we only provide the results obtained from the numerical analysis of the homoclinic orbits with the direct integration (i.e., analysis using the second method) approach. To integrate the system (6) we used a fourth-order Runge-Kutta routine. The absolute and relative errors of numerical integration did not exceed 10^{-6} and 10^{-8}, respectively. The system (6) was integrated in the region $x > 1$ from the point M^u_0 to the first intersection of the trajectory W^u_1 with the plane U_{+1}. This intersection gave us the point M^u_1. Then we calculated the deviation, d_M, of the point M^u_1 from the line l^s_μ located at the intersection between the planes $W^a_\mu(O)$ and U_{+1}. Depending upon the location of the point M^u_1 in the plane U_{+1} the deviation d_m can be either positive or negative. If $M^u_1 \in U^u_\mu$, then d_M is negative while if $M^u_1 \in U^s_\mu$, then d_M is positive. Then we varied one of the parameters of the system, for example β, and calculated the function $d_M(\beta)$, called a *splitting function*. This function shows the correspondence between the value of β and the value of the deviation d_M. An example of this function is shown in Fig. 7. The discontinuity of the splitting function (dashed line in the Fig. 7) corresponds to the approach of the trajectory W^u_1 to the

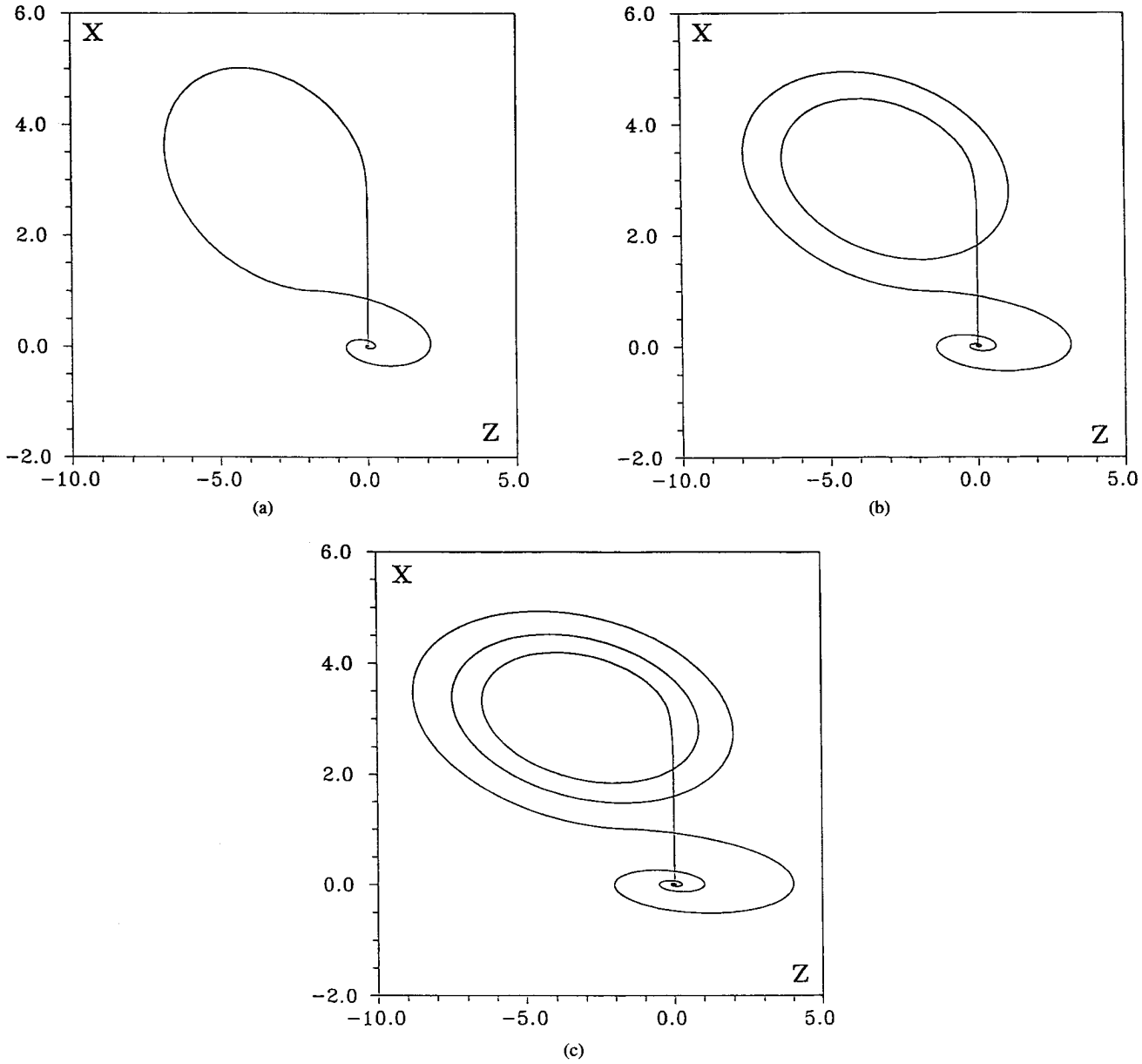

Fig. 6. Various types of homoclinic orbits of the system (6) associated with the stationary point $O(0,0,0)$. $(a),(b),(c)$, and (d) provide the homoclinic orbits which, respectively, make $n = 1$, 2, 3, and 4 rotations in the slow motion layer near the manifold $W^u_\mu(P+)$, respectively. The parameter values are $a = -2$, $b = -1/2$, $\mu = 0.01$, $\delta = 0.95$, $\gamma = 0.5$ and β, corresponding to the solid curves of bifurcation diagram (Fig. 5) labelled by $n = 1$, 2, 3, and 4, respectively.

plane U_{+1} at some point (from a small neighborhood of the point K), where the vector field of system (6) is tangent to the plane U_{+1}. The parameter value, where the splitting function crosses the zero value, corresponds to the case $M^u_1 \in l^u_\mu$ and, therefore, to the existence of a homoclinic orbit in the phase space of the system (6).

The solid lines in Fig. 5 depict the bifurcation sets Π obtained in the numerical simulations with the bifurcation value in the parameter plane (γ, β) for fixed $\mu = 0.01$, $\delta = 0.95$, $a = -2$ and $b = -\frac{1}{2}$. The index n characterizes the number of rotations made by the homoclinic orbit around the point P^+. We denote by h_n the parameter values from the bifurcation set Π corresponding to the homoclinic orbit marked by the index n. The bifurcation values obtained in the numerical simulations coincide with the approximate values of the corresponding bifurcation parameters given by (20) (dashed lines in Fig. 5). Equation (20) gives the best approximation for the homoclinic orbits with small n. The shapes of the homoclinic orbits with different index n for the parameter values from the bifurcation set Π are shown in Fig. 6. The orbits were obtained with fixed $\gamma = 0.5$ and β values taken within the bifurcation set Π (see Fig. 5).

As mentioned in Section II–B, the bifurcation set Π does not exhaust the whole bifurcation set of homoclinic orbits of the system (6). This fact can be confirmed with the analysis of the saddle-focus value, σ_{sf} of the stationary point O. The saddle-focus value is

$$\sigma_{sf} = \lambda_a + h_a$$

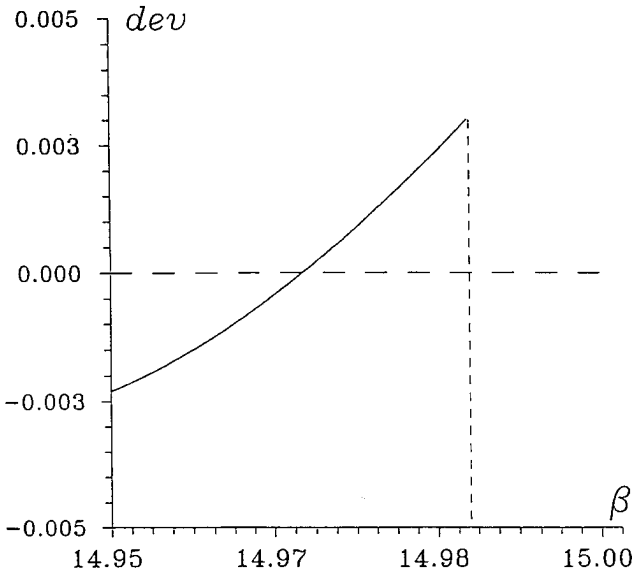

Fig. 7. The splitting function $d_M = d_M(\beta)$ calculated with $a = -2$, $b = -1/2$, $\mu = 0.01$, $\delta = 0.95$, $\gamma = 0.5$. The value of β where $d_M = 0$ corresponds to the appearance of homoclinic orbit with $n = 1$. For the homoclinic bifurcations with $n = 2, 3, \ldots$ the splitting function have a similar behavior.

where λ_a is the positive eigenvalue of the stationary point, and h_a is the real part of the complex-conjugate eigenvalues. In our case λ_a is given by (39) (Appendix B) and h_a by (43) (Appendix C). When $0 < \mu \ll 1$, the eigenvalue $\lambda_a \gg 1$ and, therefore, in our case $\sigma_{sf} > 0$. According to a theorem by Shil'nikov [20], if the saddle-focus value is positive, then other bifurcation curves corresponding to multiloop homoclinic orbits will exist in the neighborhood of the curves of the bifurcation set Π. However, they are hardly observable in numerical simulations. Indeed when $\lambda_a \gg 1$, the plane $W^s_\mu(O)$ is strongly unstable and any incoming trajectory to the slow motion layer near $W^s_\mu(O)$ rapidly leaves this layer. This instability in the transition from slow motions to fast motions causes stiffness of the system (6). When $\mu = 0.1$ the situation is easier and mutliloop homoclinic orbits may be observed in the numerical simulations. Such homoclinic orbits are generated by the trajectory W^u_1 in the following way. At the first intersection of the plane U_{+1} (from the region $x > 1$) the trajectory gets into the region U^s_μ (see Fig. 4 (b) and (a)), moves in the slow motion layer above the plane $W^s_\mu(O)$, and at the second intersection with U_{+1} (from the region $x > 1$) the trajectory gets into the l^s_μ and forms the homoclinic orbit.

C. Homoclinic Orbits. Physical Experiment

We have also studied homoclinic orbits in experiments with electronic circuits (see Fig. 8). To observe the (v_1, v_2)-projections of the trajectories of the circuit, the voltages v_1 and v_2 are applied to the "X" and "Y" terminals of the oscilloscope. A periodic pulse generated by a function generator is used to periodically set the initial state of the circuit near the stationary point O by short-circuiting the nonlinear active element N_R with a relay. This short-circuiting makes the origin in the resulting system asymptotically stable. The pulses from the function generator are also used for intensity modulation (via

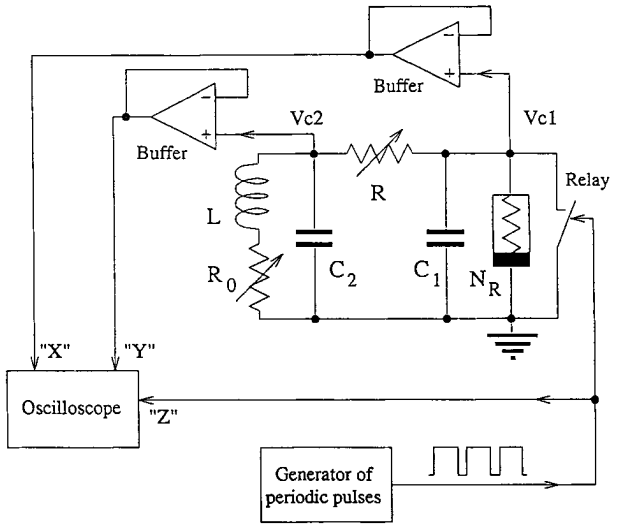

Fig. 8. Schematic diagram of the experimental setup for generating pictures of homoclinic orbits.

the "Z" terminal of the oscilloscope) to display the intervals of the trajectories starting from the vicinity of the stationary point O and ending when the relay is switched on. As it follows from Section II–A the behavior of the trajectories originating from O changes qualitatively when the parameters of the circuit cross the bifurcation values of the parameters where the system has homoclinic orbits. This qualitative change of the trajectory is used to detect the transition of the circuit through homoclinicity. For earlier use of this and other techniques for the same problem (see [21] through [23]).

In our experiments we use the OP AMP implementation of the circuit proposed by Kennedy [24]. The state equations of the circuit are [25], [26]

$$\begin{cases} C_1 \frac{dv_1}{dt} &= G(v_2 - v_1) - g(v_1), \\ C_2 \frac{dv_2}{dt} &= G(v_1 - v_2) + i_L, \\ L \frac{di_L}{dt} &= -v_2 - R_0 i_L \end{cases} \tag{22}$$

where $G = 1/R$ and the nonlinear function $g(v_1)$, which defines the $v - i$ characteristic of the nonlinear active element N_R, is described by the piecewise-linear function

$$g(v_1) = m_0 v_1 + \frac{1}{2}(m_1 - m_0)[|v_1 + B_p| - |v_1 - B_p|]. \tag{23}$$

In our experimental setup, we fixed $m_1 = -0.5mS$, $m_0 = -0.11mS$, and $B_p = 0.5V$. We also fixed the linear elements of the circuit at $L = 129mH$, $C_1 = 1nF$, and $C_2 = 47nF$. The values of the resistors R and R_0 are used as control parameters of the dynamics of the circuit. The bifurcations found associated with homoclinic orbits are given in Fig. 9. These bifurcation curves are coded by the indices h_n. When the parameters of the circuit are chosen from the bifurcation curve h_n, the homoclinic trajectory starts at the unstable stationary point O, goes to the plane of slow motions, makes n rotations around the stationary point P^+ and then returns back to O.

As it follows from the analysis of the homoclinic bifurcations the behavior of the trajectory originating at the stationary

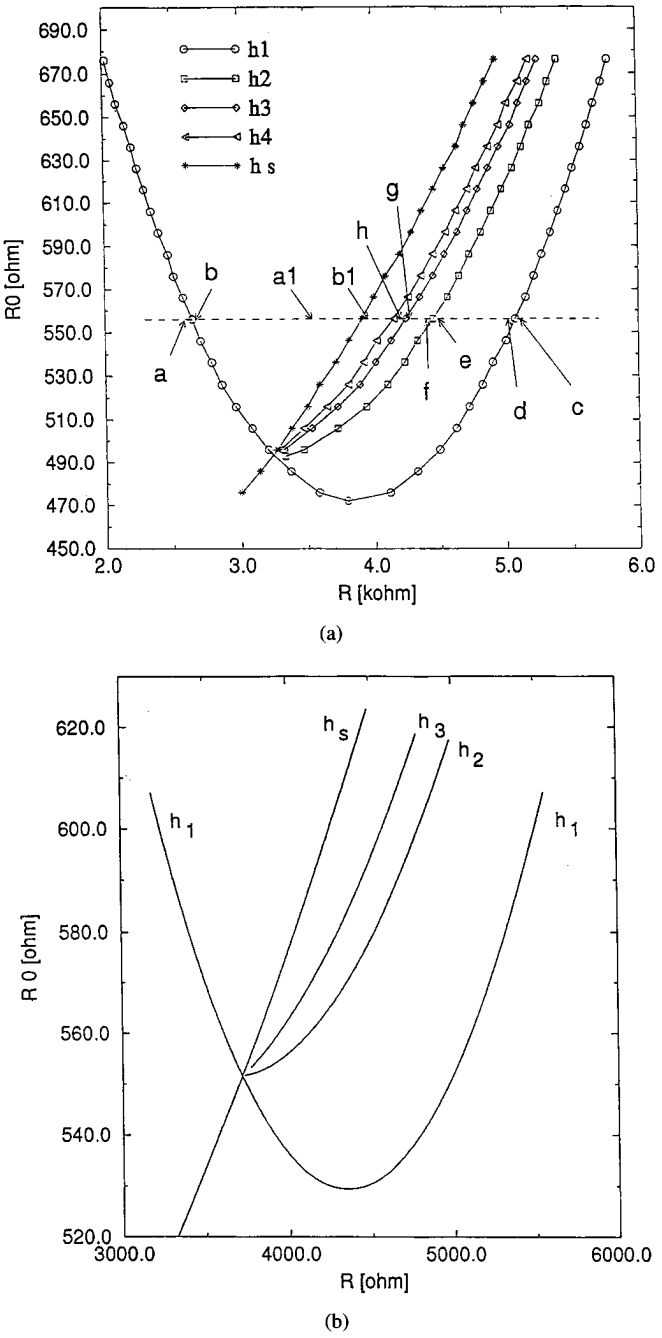

Fig. 9. The bifurcation diagram in the plane of physical parameters (R, R_0). (a) Bifurcation curves measured in the experiment with the circuit. (b) Bifurcation curves obtained in the numerical simulations of the system (6) when the parameters of the system are the same as in the experiment (a).

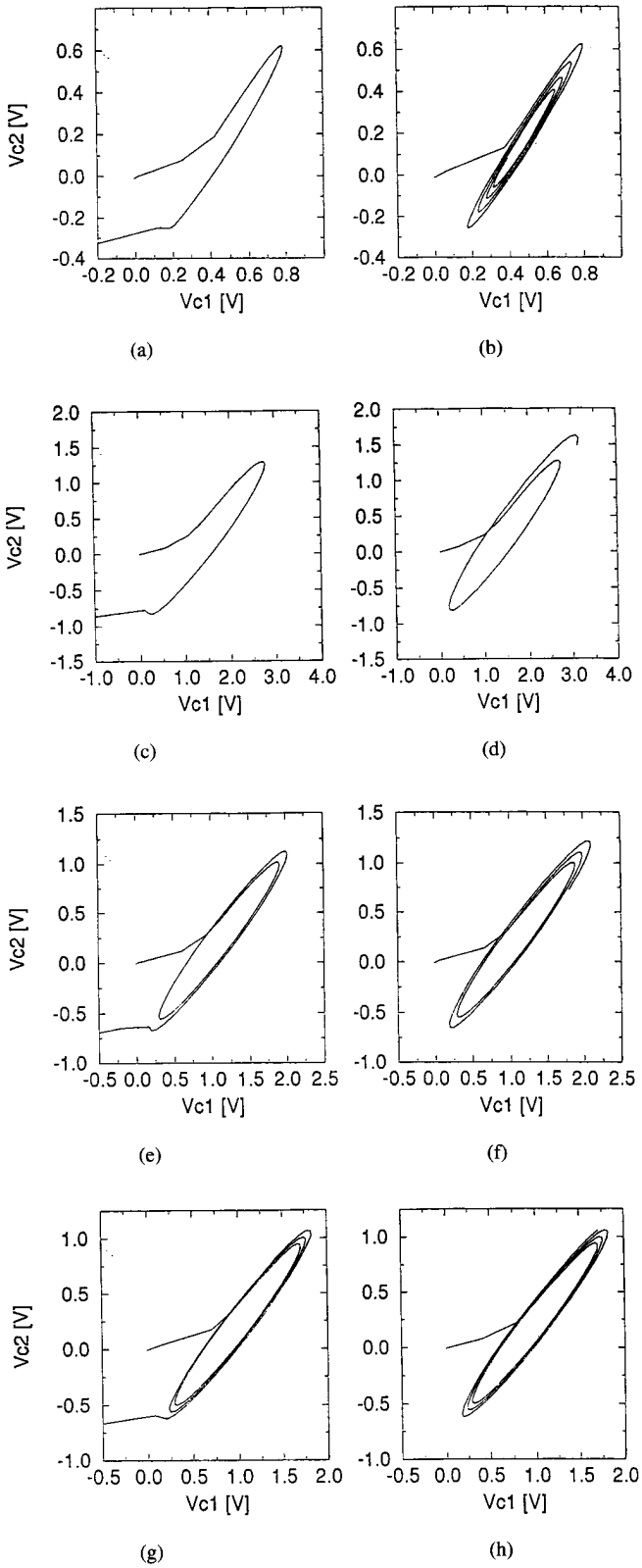

Fig. 10. The behavior of the trajectory originating at the stationary point O in the experiment with the circuit. The parameter values of the circuit were taken close to the homoclinic bifurcation. The trajectories shown in (a)–(h) were measured with the values used for Fig. 9(a) identified by arrows with corresponding labels.

hyperbolic point changes qualitatively when the parameters of the circuit cross the bifurcation values associated with the homoclinicity. Consider the behavior of the trajectory studied in the experiment with $R_0 = 556\Omega$. We have observed two different types of bifurcation associated with the homoclinic orbit h_1. The first type has been observed in the parameter region where the stationary point P^+ is stable. Fig. 10(b) shows the trajectory obtained when the parameters of the circuit are chosen in the region above the left branch of the bifurcation curve h_1, where the stationary point P^+ is stable. The trajectory starts from O goes to the manifold of slow motions and then is attracted by the stable stationary point P^+. After the bifurcation, when the parameters of the circuit

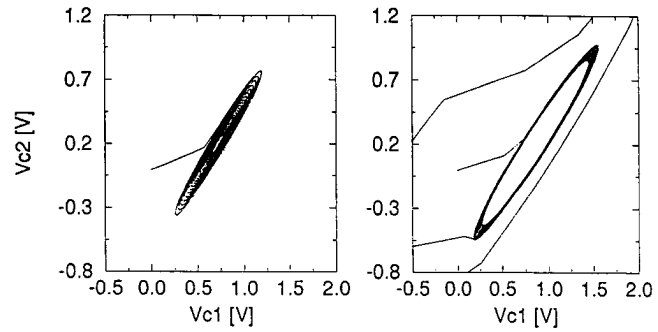

Fig. 11. The behavior of the trajectory originating from the stationary point O. The parameters of the measurements (a) and (b) are those used for Fig. 9(a) identified by arrows with the labels $a1$ and $b1$, respectively.

are below the curve h_1 the trajectory starting at O, goes to the manifold of slow motions, makes one rotation around P^+, then falls from the plane of slow motions and travels fast to the other branch of the manifold of slow motions associated with the stationary point P^-. This trajectory is shown in Fig. 10(a).

The second type of bifurcation is observed in the parameter region where both stationary points P^+ and P^- are unstable. After the homoclinic bifurcation the trajectory behaves similarly to the trajectory measured after the bifurcation of the first type, as comparison of Fig. 10(a) and (c) shows. However, before bifurcation the behavior of the trajectory is different from the trajectory measured before the bifurcation of the first type. Now it is not attracted by P^+ because this stationary point is no longer stable. In this case, the trajectory makes a second rotation in the slow motion layer near the manifold $W^u_\mu(P+)$ diverging from the stationary point P^+ and then falls from the manifold, as illustrated in Fig. 10(d).

In the experiment we have observed that the homoclinic orbits h_n, with $n > 1$, appear only with bifurcations of the second type. The trajectories measured in the vicinity of higher–order homoclinicity are shown in Fig. 10 (e)–(h).

As mentioned earlier, the existence of two different types of homoclinic bifurcations h_1 originates from the change of stability properties of the stationary point P^+. The parameter regions corresponding to different types of bifurcation are divided by the bifurcation curve h_s where P^+ losses stability. Fig. 11(a) and (b) shows the behavior of the trajectories originating from O, and measured before and after the point P^+ losses its stability.

III. Solitary Waves

As indicated in the Introduction, the appearance of homoclinic orbits in the phase space of the system (6) indicates the existence of solutions of the system (2), (3) in the form of *solitary waves*. The parameters of the solitary waves depend on the parameter values on the bifurcation set II. The wave profiles correspond to the forms of the homoclinic orbits as discussed in Section II. The number of pulses in the solitary wave profile is determined by the number of rotations of the homoclinic orbits both around the stationary point P^+ and around the stationary point O (see Fig. 6). Since the stationary

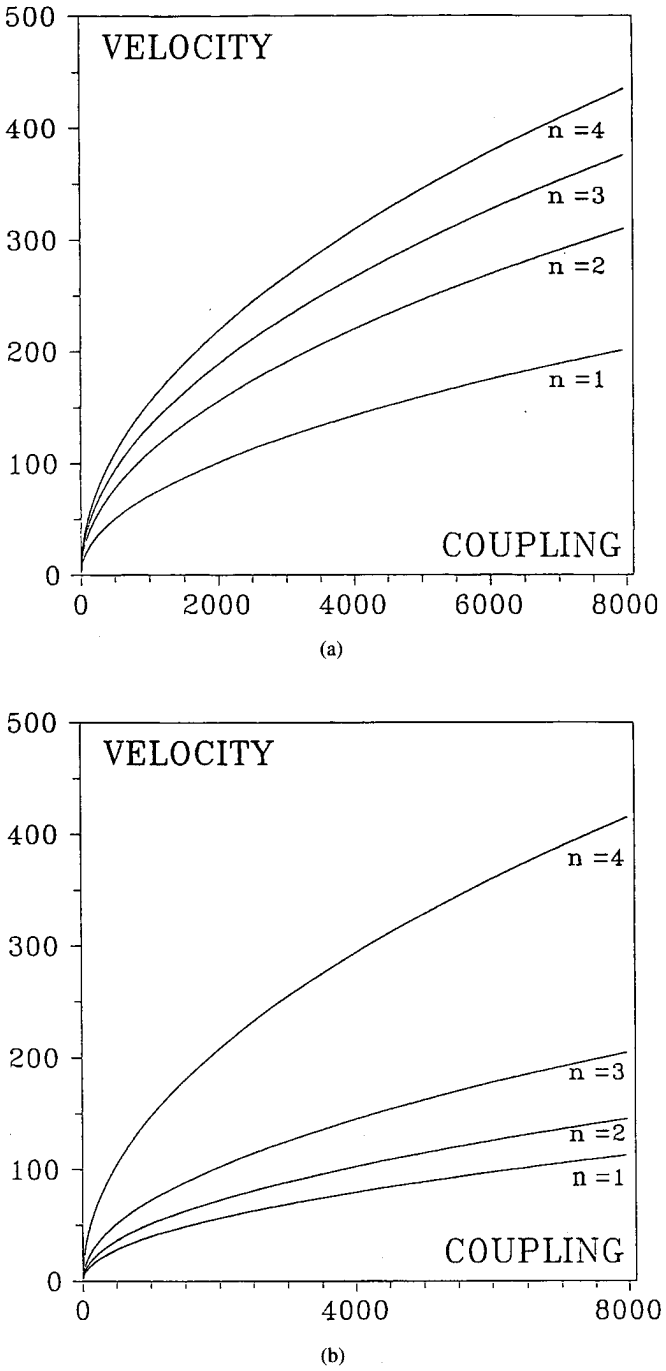

Fig. 12. Solitary wave velocity c as a function of the coupling parameter d with fixed parameter values $a = -2$, $b = -1/2$, $\mu = 0.01$, $\delta = 0.95$. (a) $\gamma = 0.95$, $\beta = 9$, (b) $\gamma = 0.5$, $\beta = 45$. The index n provides the number of humps of the solitary wave.

point O is of a saddle-focus type, the profiles of the solitary waves contain oscillating, wavy tails.

Let us see the characteristics of the possible solitary wave solutions in the system (2), (3) as a function of the coupling parameter. The dependence of the velocities of the solitary wave solutions of the system (2), (3) upon the coupling parameter are shown in Fig. 12(a) and (b). The values were obtained for two different parameter sets (β, γ, μ). To find the values of parameter δ corresponding to the existence of the solitary waves we examined the splitting function described

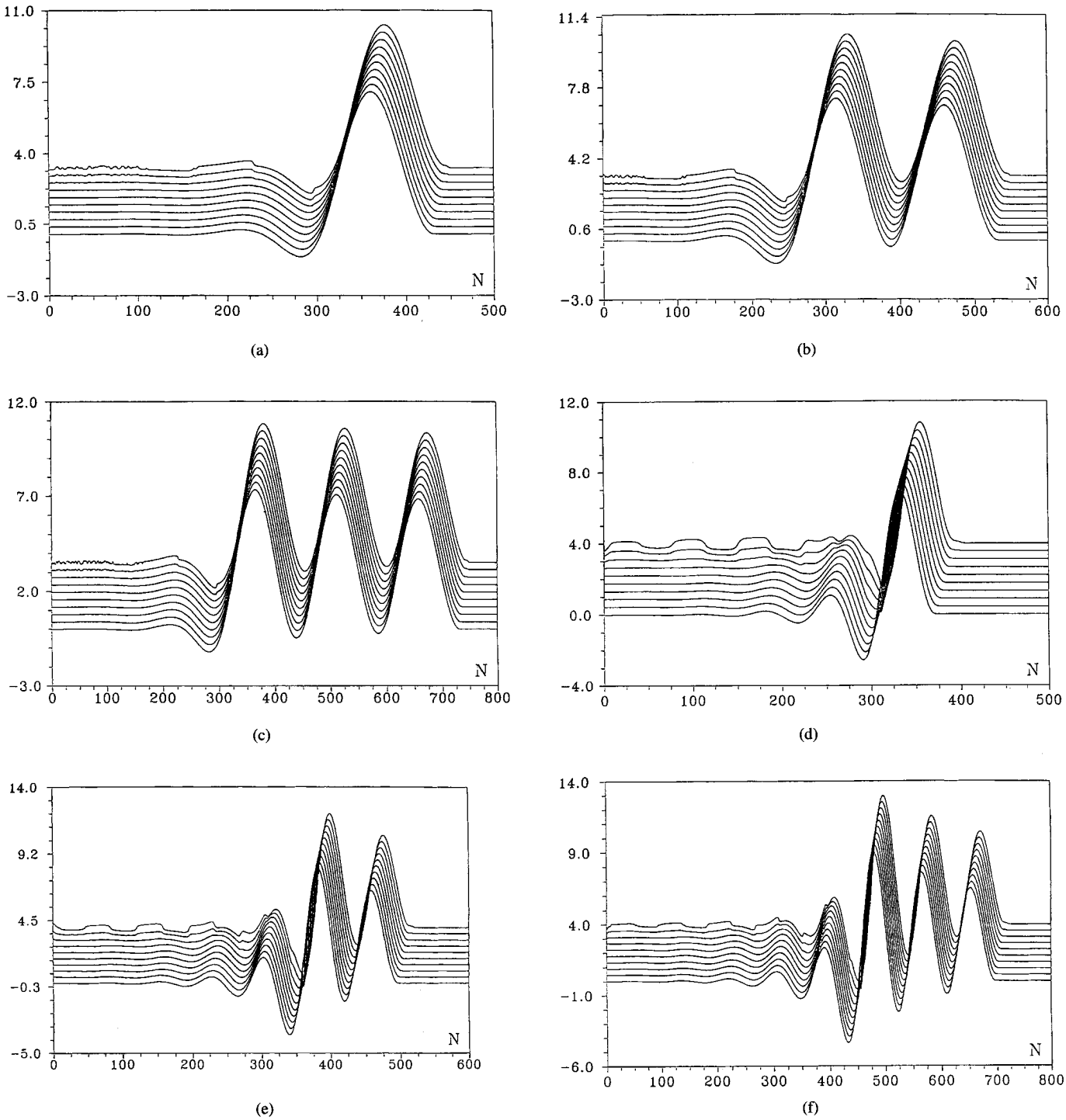

Fig. 13. Evolution of solitary waves. The "x"-coordinate corresponds to the "spatial" coordinate j, the "y"-coordinate to the value $-z + s\tau$, with z being the dimensionless coordinate proportional to the current through the inductor L. τ is the dimensionless time and s is a scaling coefficient. The parameter values in the array are $a = -2$, $b = -1/2$, $\mu = 0.01$. (a) $\gamma = 0.95$, $\beta = 9$, $d = 662.067$, $c = 66.667$, $s = 15$. The final time of integration $t_{end} = 0.234$. (b) $\gamma = 0.95$, $\beta = 9$, $d = 208.937$, $c = 50$, $s = 15$, $t_{end} = 0.234$. (c) $\gamma = 0.95$, $\beta = 9$, $d = 252.996$, $c = 66.667$, $s = 15$, $t_{end} = 0.234$. (d) $\gamma = 0.5$, $\beta = 45$, $d = 9995$, $c = 125$, $s = 20$, $t_{end} = 0.18$. (e) $\gamma = 0.5$, $\beta = 45$, $d = 3876.1$, $c = 100$, $s = 20$, $t_{end} = 0.18$. (f) $\gamma = 0.5$, $\beta = 45$, $d = 1971.5$, $c = 100$, $s = 20$, $t_{end} = 0.18$.

in Section II–B with argument δ. We have

$$c^2 = \frac{d}{1 - \delta_n}$$

where δ_n are the values of δ corresponding to the appearance of homoclinic orbits of the system (6) with index n. The propagation of such solitary waves in the array depends on their stability. Two different approaches have been taken in studying stability. In the numerical simulations we have investigated the initial value problem with data close to the solitary wave solution (see Fig. 13 and the discussion below). The other approach follows the criteria used in the theory

of continuously distributed systems, where the stability of a spatially homogeneous state associated with the solitary wave may be used as one of the conditions for stability of the solitary wave. In the case of an array (i.e., a discrete medium) this condition should be satisfied too. It is shown in Appendix D that all homogeneous stationary states of the system (2), (3) are unstable. Therefore, strictly speaking, all solitary waves in the array (2), (3) are unstable. However, if instability does not set in too fast, or too strongly, the possible solitary waves may actually occur and propagate for quite a long time interval before any appreciable change is seen. Then we may very well speak of a long time "practical" stability of the waves which show slow enough "aging" effects.[5] In numerical simulations of the system (2) we have found that there are parameter values such that solitary waves can propagate rather far with only slight changes of their profile.

The evolution of the initial wave profiles chosen close to the solitary waves solutions is illustrated in Fig. 13. Fig. 13(a), (b), and (c) shows the evolution of solitary waves propagating with the velocities given in Fig. 12(a). Fig. 13(d), (e), and (f) corresponds to the velocities given in Fig. 12(b). The "x"-axis in Fig. 13 corresponds to the "spatial" coordinate j, while the "y"-axis corresponds to $z + s\tau$, where τ is a dimensionless time and s is a scaling coefficient. Fig. 13 shows to what extent can solitary waves of different shape propagate with no appreciable changes. However, the oscillating tail of the waves affects the unstable stationary state ($x_j = y_j = z_j = w_j = 0$) and indeed after some time interval small perturbations will develop in the background of the solitary wave (Fig. 13). These perturbations finally grow strong enough to finally destroy the solitary waves. Notice that the scale of the instability is different for different parameter sets. In particular, if the coupling parameter is large (Fig. 13(d), (e), and (f)) the scale of the instability is also large.

IV. Concluding Remarks

Our study naturally falls in two parts. The first part deals with the spatio-temporal dynamics of an array of identical oscillators modelled by Chua's circuit. We have shown that when a group of such circuits are inductively coupled to form a one-dimensional array, solitary waves are possible for certain parameter values. These solitary waves may have a single hump or they may show a rather complicated form with two, three, and more humps. We have analyzed the dependence of their (phase) velocity on the coupling parameter. We have also shown that strictly speaking they are unstable. However, our numerical simulations showed that they can nevertheless propagate with no appreciable change of profile for quite some time. Hence a one-dimensional array of inductively coupled Chua's circuits may be considered as a nonequilibrium "medium" with properties similar to the properties of dissipative continuous media as for instance cases where the evolution is describable by a dissipation-modified Korteweg–de Vries equation (KdVE). Two such cases are the Marangoni-Benard convection when a liquid layer is heated from above and the evolution of internal waves in some sheared, stably stratified fluid layers. Thus a conclusion is that besides their intrinsic value and its potential electronic telecommunication applicability, experiments with one-dimensional arrays of Chua's circuits may help in our understanding of the qualitative properties of these and other hydrodynamic processes in the atmosphere, or the oceans, as well as in other fields of science and technology where dissipation and nonlinearity are key elements acting together.

The second part of our report deals with the individual dynamics of Chua's circuit. We have studied the bifurcation set Π corresponding to the appearance of homoclinic orbits associated with the stationary point O at the origin of the phase space of the circuit. In the parameter plane (β, γ) the set Π represents the bundle of curves originating from the same point Π_0. We have shown that the saddle value of the saddle-focus O is positive, hence in the neighborhood of bifurcation set Π there exits a countable set of bifurcation curves corresponding to homoclinic orbits with any numbers of loops.

Appendix A
Integral Manifolds of Stationary Points

Consider the system (6) in the region $-1 \le x \le 1$

$$\begin{cases} \mu\dot{x} = y - x - (1+a)x, \\ \delta\dot{y} = x - y + z, \\ \dot{z} = -\beta y - \gamma z. \end{cases} \tag{24}$$

The system (24) has a single stationary point O at the origin. Its corresponding characteristic equation is

$$\lambda^3 + \left[\gamma + \frac{1}{\delta} + \frac{a+1}{\mu}\right]\lambda^2 + \left[\frac{\gamma+\beta}{\delta} + \frac{\gamma(a+1)}{\delta} + \frac{a}{\mu\delta}\right]\lambda + \frac{\beta(a+1)}{\mu\delta} + \frac{\gamma a}{\mu\delta} = 0. \tag{25}$$

Then within the G_u parameter region (defined by conditions (8)), equation (25) has one positive root $\lambda = \lambda_a$ and a pair of complex conjugate roots. Therefore the stationary point O is a saddle-focus with a one-dimensional unstable manifold $W^u_{1,2}$ and a stable separatrix plane $W^s_\mu(O)$. Let us derive the equations which describe these manifolds. To define $W^s_\mu(O)$ we change variables from (x, y, z) to (u_1, u_2, u_3) via the transformation

$$\begin{bmatrix} x \\ y \\ z \end{bmatrix} = \begin{bmatrix} 1 & -k_1^a & -k_2^a \\ 0 & 1 & 0 \\ 0 & 0 & 1 \end{bmatrix} \begin{bmatrix} u_1 \\ u_2 \\ u_3 \end{bmatrix} \tag{26}$$

with

$$\begin{aligned} k_1^a &= \delta(\lambda_a + \tfrac{a+1}{\mu}) \\ k_2^a &= \frac{1}{\beta}\{-\tfrac{a}{\mu} - [1 + \tfrac{\delta(a+1)}{\mu}]\lambda_a - \delta\lambda_a^2\}. \end{aligned} \tag{27}$$

Then the system (24) becomes

$$\begin{cases} \dot{u_1} = \lambda_a u_1 \\ \dot{u_2} = \frac{1}{\delta}u_1 - \frac{k_1^a+1}{\delta}u_2 - \frac{k_2^a-1}{\delta}u_3 \\ \dot{u_3} = -\beta u_2 - \gamma u_3. \end{cases} \tag{28}$$

It follows from the first equation of (28) that in the new phase variables (u_1, u_2, u_3) the separatrix plane $W^s_\mu(O)$ is given by

[5] Such "practical" stability has been advocated in studies of a dissipation-modified Korteweg-de Vries equation modeling at least qualitative features of oscillatory Benard-Marangoni convection [10], [11].

the equation $u_1 = 0$. Therefore, taking into account (26), the equation of the separatrix plane in the phase space (x, y, z) is

$$W^s_\mu(O): \left\{x + \delta(\lambda_a + \tfrac{a+1}{\mu})y + \tfrac{1}{\beta}[-\tfrac{a}{\mu} - [1 + \tfrac{\delta(a+1)}{\mu}]\lambda_a - \delta\lambda_a^2]z = 0\right\}. \tag{29}$$

Hence motions on the plane $W^s_\mu(O)$ are governed by the 2-dimensional system

$$\begin{cases} \dot{y} = -\dfrac{k_1^a + 1}{\delta}y - \dfrac{k_2^a - 1}{\delta}z \\ \dot{z} = -\beta y - \gamma z \end{cases} \tag{30}$$

To derive the equations of the one-dimensional manifold $W^u_{1,2}$, we now change variables in the form

$$\begin{bmatrix} x \\ y \\ z \end{bmatrix} = \begin{bmatrix} -k_4^a & 0 & 1 \\ 1 & 0 & 0 \\ 1 + k_4^a - k_3^a & 1 & -1 \end{bmatrix} \begin{bmatrix} v_1 \\ v_2 \\ v_3 \end{bmatrix} \tag{31}$$

where

$$\begin{aligned} k_3^a &= -\lambda_a\delta \\ k_4^a &= -\frac{1}{\lambda_a\mu + a + 1}. \end{aligned} \tag{32}$$

Then with the variables (v_1, v_2, v_3) the system (24) becomes

$$\begin{cases} \dot{v_1} = \lambda_a v_1 + \frac{1}{\delta}v_2 \\ \dot{v_2} = [-\gamma - \frac{(1+\lambda_a\delta)}{\delta}]v_2 + [\gamma - \frac{a+1}{\mu}]v_3 \\ \dot{v_3} = -\frac{1}{\delta(\lambda_a\mu + a + 1)}v_2 - \frac{(a+1)}{\mu}v_3. \end{cases} \tag{33}$$

The unstable one-dimensional manifold is given by the equations $v_2 = 0, v_3 = 0$. In terms of the original variables (x, y, z) it can be represented as

$$W^u_\mu(O): \left\{-\frac{x}{k_4^a} = \frac{y}{1} = \frac{z}{1 + k_4^a - k_3^a}\right\}. \tag{34}$$

A similar approach permits us to derive the equations of the integral manifolds of the stationary points $P^\pm$. Their corresponding characteristic equations can be written in the form (25) using the substitution $a \to b$. Both stationary points $P^\pm$ have one negative eigenvalue $\lambda = \lambda_b$ and two complex-conjugate eigenvalues $\lambda = h_b \pm i\omega_b$. In the parameter region G_u (see Fig. 2) h_b is positive, and in the region G_s this h_b is negative. Therefore, these stationary points are either asymptotically stable points (in the region G_s), or saddle-foci with $dim\ W^s_\mu(P^\pm) = 1$ and $dim\ W^u_\mu(P^\pm) = 2$, respectively. The equations describing these manifolds are

$$\begin{aligned} W^u_\mu(P^\pm): &\left\{x \mp x_0 + \delta\left(\lambda_b + \tfrac{b+1}{\mu}\right)(y \mp y_0)\right. \\ &\left. + \frac{1}{\beta}\left[-\frac{b}{\mu} - [1 + \tfrac{\delta(b+1)}{\mu}]\lambda_b - \delta\lambda_b^2\right](z \mp z_0) = 0\right\} \end{aligned} \tag{35}$$

$$W^s_\mu(P^\pm): \left\{-\frac{x \mp x_0}{k_4^b} = \frac{y \mp y_0}{1} = \frac{z \mp z_0}{1 + k_4^b - k_3^b}\right\} \tag{36}$$

where $k_1^b, k_2^b, k_3^b, k_4^b$ are defined by the formulas (27) and (32) using the substitution $\lambda_a \to \lambda_b$.

Appendix B
Relative Location of the Manifolds $W^s_\mu(O)$ and $W^u_\mu(P^+)$

It follows from (29) and (30) that the lines at the intersection of the manifolds $W^s_\mu(O)$, $W^u_\mu(P_+)$ with the plane U_{+1} are given by

$$\begin{aligned} l^s_\mu &: \{k_1^a y + k_2^a z + 1 = 0\} \\ l^u_\mu &: \{k_1^b(y - y_0) + k_2^b(z - z_0) + 1 - x_0 = 0\} \end{aligned} \tag{37}$$

respectively.[6] Since $\frac{k_1^a}{k_1^a} \neq \frac{k_1^b}{k_1^b}$, the lines l^s_μ, l^u_μ intersect each other in some point $L(y_l, z_l)$. Therefore, in the phase space of the system (6) there exists a trajectory Γ_l which contains this point and simultaneously belongs to both manifolds $W^s_\mu(O)$, $W^u_\mu(P^+)$. As $\xi \to +\infty$ the trajectory Γ_l tends to the point O, and as $\xi \to -\infty$ to the point P^+. Using (37) the coordinates of the point L can be written as

$$y_l = \frac{\Delta_1}{\Delta}\ ,\ z_l = \frac{\Delta_2}{\Delta}$$

where

$$\begin{aligned} \Delta &\equiv k_1^a k_2^b - k_1^b k_2^a \\ \Delta_1 &\equiv -k_2^b - k_2^a(x_0 - 1 + k_1^b y_0 + k_2^b z_0) \\ \Delta_2 &\equiv k_1^b + k_1^a(x_0 - 1 + k_1^b y_0 + k_2^b z_0). \end{aligned} \tag{38}$$

Note that in (38) the coordinates $(y_l,\ z_l)$ are given by the parameters of the system (6) (see Appendix A) and by the eigenvalues λ_a and λ_b. To make $(y_l,\ z_l)$ depend only on the parameters of the system (6), we use an asymptotic representation of the eigenvalues λ_a and λ_b

$$\lambda_q = -\frac{q+1}{\mu} - \frac{1}{\delta(q+1)} + \sum_{k=1}^{4}\Psi_k^q\mu^q + O_q(\mu^5) \tag{39}$$

where the index q stands for either a, or b, and the values Ψ_k^q are given by the following expressions:

$$\begin{aligned} \Psi_1^q &\equiv -\frac{q}{\delta^2(q+1)^3}\ ,\ \Psi_2^q \equiv -\frac{q(q-1)}{\delta^3(q+1)^5} + \frac{\beta}{\delta^2(q+1)^3} \\ \Psi_3^q &\equiv -\frac{q(1 - 3q + q^2)}{\delta^4(q+1)^7} + \frac{\gamma\beta}{\delta^2(q+1)^4} - \frac{2\beta(1-q)}{\delta^3(q+1)^5} \\ \Psi_4^q &\equiv \frac{q(1-q)(1-5q+q^2)}{\delta^5(q+1)^9} - \frac{\gamma\beta(3-2q)}{\delta^3(q+1)^6} \\ &\quad + \frac{3\beta(1-3q+q^2)}{\delta^4(q+1)^7} + \frac{\gamma^2\beta}{\delta^2(q+1)^5} - \frac{\beta^2}{\delta^3(q+1)^5}. \end{aligned}$$

Using (39), (27), and (38) we obtain the following coordinates of the point L:

$$\begin{aligned} y_l &= (a+1)\{1 - \frac{[\gamma a + \beta(a+1)]}{a(a+1)^2(b+1)}\mu^2 + O(\mu^3)\} \\ z_l &= a\{1 - \frac{[\gamma a + \beta(a+1)](a+b+2)}{a(a+1)(b+1)}\mu + \\ &\frac{[\gamma a + \beta(a+1)]}{a(a+1)(b+1)}\left[\gamma + \frac{(a+1)^3 + (b+1)^3}{\delta(a+1)^2 - (b+1)^2}\right]\mu^2 + O(\mu^3)\}. \end{aligned} \tag{40}$$

Note that since the values Δ, $\Delta_1, and\ \Delta_2$ in (38) are of the order of μ, we have used the asymptotic representation of λ_a

[6]Note that in the case of $\mu = 0$ these lines become a single one $l_0 : \{y = a + 1\}$.

and λ_b with an accuracy up to μ^4 in order to get $(y_l,\ z_l)$ with an accuracy of μ^2.

Appendix C
Flow Trajectories on the Manifolds $W^s_\mu(O)$ and $W^u_\mu(P^+)$

Let us obtain the coordinates of the points M and K which are located on the lines l^s_μ and l^u_μ, respectively. These points are used as the boundaries dividing the flow located on the planes $W^s_\mu(O)$ and $W^u_\mu(P^+)$ into incoming and outgoing trajectories from these planes.

Let us start with the analysis of the trajectory behavior on the plane $W^s_\mu(O)$. This behavior is described by the system of two differential equations (30). In order to study the orientation of the vector field (30) on the line $l^s_\mu = W^s_\mu(O) \cap U_1$ we consider the function

$$w = k^a_1 y + k^a_2 z + 1$$

and its derivative with respect to (30). Then we apply the condition

$$\dot{w}\,|_{w=0} = 0,$$

which is used to define the coordinates of the point $M(y_m, z_m)$. This point belongs to the line l^s_μ and divides the flow located on the manifold $W^s_\mu(O)$ into incoming and outgoing trajectories from the plane $W^s_\mu(O)$. The coordinates of the point M are

$$y_m = (a+1) + O(\mu^3)$$

$$z_m = a - \frac{[\beta(a+1)+\gamma a]}{(a+1)}\mu + \frac{[\beta(a+1)+\gamma a]}{\delta(a+1)^3}\mu^2 + O(\mu^3). \tag{41}$$

Hence, the vector field orientation of the system (6) along the line l^s_μ is the following:

- In the interval $z > z_m$ it is directed at the decreasing values of the x-coordinate.
- In the interval $z < z_m$ it is directed at the increasing values of the x-coordinate.
- At the point $z = z_m$ it is tangent to the plane U_1.

Using a similar technique we can obtain the coordinates of the point K which belongs to the line l^u_μ. At point K the flow located on the plane $W^u_\mu(P^+)$ are divided into incoming and outgoing trajectories. The coordinates of the point K are

$$y_k = (a+1) + O(\mu^3)$$

$$z_k = a - \frac{[\beta(b+1)+\gamma b]}{(b+1)}\mu + \frac{[\beta(b+1)+\gamma b]}{\delta(b+1)^3}\mu^2 + O(\mu^3). \tag{42}$$

In the remaining part of this Appendix we describe the properties of the trajectories lying on the manifold $W^u_\mu(P^+)$. It follows from (30), (32), and (39) that motions on $W^u_\mu(P^+)$ in the region $x \geq 1$ are governed by the following system of the differential equations:

$$\begin{cases} \dot{y} = \frac{B_\mu}{\delta} y + \frac{I_\mu}{\delta} z + \frac{D_\mu}{\delta} \\ \dot{z} = -\beta y - \gamma z \end{cases} \tag{43}$$

where (see equations at the bottom of this page). The system (43) has a stationary point with coordinates $(y_0,\ z_0)$ (see (9)). Its corresponding eigenvalues are

$$\lambda_{1,2} = -h_b \pm i\omega_b \tag{44}$$

with

$$h_b \equiv \frac{(\gamma - \frac{B_\mu}{\delta})}{2}$$

$$\omega_b \equiv \sqrt{\frac{I_\mu \beta}{\delta} - \frac{(\gamma + \frac{B_\mu}{\delta})^2}{4}}.$$

The analysis of these eigenvalues shows that in the parameter region G_u (see Fig. 2) the stationary point $(x_0,\ y_0)$ is an unstable focus ($h_b < 0$), but within the region G_s it is a stable focus ($h_b > 0$).

Appendix D
Instability of the Spatially Homogeneous States

In Section III we discussed the instability of the spatially homogeneous solution associated with the homoclinic orbit as one of the criteria for instability of the solitary waves. In this appendix we illustrate the instability of the spatially homogeneous solution of the system (2) using the following boundary conditions:

$$\begin{aligned} y_{N+1} &= y_N \\ w_0 &= w_1. \end{aligned} \tag{45}$$

Consider the stationary poins of the system (2), (45) which are contained in the region $|x_j| \leq 1,\ (j = 1, 2, \ldots, N)$. The stationary states of the array correspond to these stationary points. Then in the region $|x_j| \leq 1$ the system (2)–(45) has a one-parameter family of stationary states. This family is given as

$$\{x_j = y_j = z_j = 0,\ w_j = w_0 = const\}$$

$$j = 1, 2, \ldots, N.$$

$$B_\mu \equiv B\left\{1 - \frac{\mu}{\delta(b+1)^2} + \left[\frac{1-b}{\delta^2(b+1)^4} + \frac{\beta}{\delta b(b+1)^2}\right]\mu^2 + O(\mu^3)\right\}$$

$$I_\mu \equiv 1 - \frac{\mu}{\delta(b+1)^2} - \left[\frac{\gamma}{\delta(b+1)^3} - \frac{(1-b)}{\delta^2(b+1)^4}\right]\mu^2 + O(\mu^3)$$

$$D_\mu \equiv D\left\{1 - \frac{\mu}{\delta(b+1)^2} + \frac{(1-b)}{\delta^2(b+1)^4}\mu^2 + O(\mu^3)\right\}.$$

To examine the stability of these states we analyze the characteristic determinant (see matrix at the bottom of the page), where $\sigma \equiv -\alpha(1+a)$. Expanding Q_N along the first four rows, we rewrite it in the form

$$Q_N = q_1 A_{N-1} + q_2 B_{N-1} \tag{46}$$

where A_{N-1}, B_{N-1} are some determinants, and

$$q_1 \equiv \lambda^4 + [1+\gamma+\alpha(1+a)]\lambda^3 + [\alpha a+\alpha(1+a)\gamma+\gamma+\beta]\lambda^2+\alpha[a\gamma+(1+a)\beta]\lambda$$

$$q_2 \equiv \frac{dq_1}{\lambda}.$$

Next, let us expand the determinant A_{N-1} along the first four rows to obtain

$$A_{N-1} = q_3 A_{N-2} + q_2 B_{N-2} \tag{47}$$

where

$$q_3 \equiv q_1 - \epsilon,$$
$$\epsilon \equiv d(\sigma-\lambda)(\gamma+\lambda).$$

On the other hand, expanding the determinant A_{N-1} along the last four rows we obtain

$$A_{N-1} = q_1 S_{N-2} - \lambda\frac{\epsilon}{d} C_{N-2} \tag{48}$$

where the determinants S_{N-2} and C_{N-2} have the following forms (see matrix at the bottom of the next page). Then we expand the determinants S_{N-2} and C_{N-2} along the last four rows and obtain

$$\begin{aligned} S_{N-2} &= q_3 S_{N-3} - \tfrac{\lambda\epsilon}{d} C_{N-3} \\ C_{N-2} &= q_2 S_{N-3} - \epsilon C_{N-3} \end{aligned} \tag{49}$$

It follows from (49) that

$$C_{N-2}\lambda = d(q_1 - q_3)S_{N-3} + dS_{N-2}. \tag{50}$$

From (48) and (50) we obtain

$$A_{N-1} = (q_1-\epsilon)S_{N-2} - \epsilon^2 S_{N-3}. \tag{51}$$

Finally, from (51), (47), and (46) we find

$$Q_N = (q_1-\epsilon)S_{N-1} + \epsilon(q_1-2\epsilon)S_{N-2} - \epsilon^3 S_{N-3}. \tag{52}$$

The Lyapunov characteristic eigenvalues corresponding to the stationary homogeneous states are defined by the following equation:

$$(q_1-\epsilon)S_{N-1} + \epsilon(q_1-2\epsilon)S_{N-2} - \epsilon^3 S_{N-3} = 0. \tag{53}$$

On the other hand, from (50) and (51) we obtain the following recurrent relation

$$S_{N-1} = 2z\epsilon S_{N-2} - \epsilon^3 S_{N-3} \tag{54}$$

where

$$2z\epsilon \equiv q_1 - 2\epsilon.$$

Using the technique already applied in [5] and [14] we treat the recurrent relation (54) as a two-dimensional mapping with the initial conditions

$$\begin{aligned} S_1 &= \epsilon(2z+1) \\ S_2 &= \epsilon^2(4z^2+2z-1). \end{aligned} \tag{55}$$

Solving (54) and (55) we obtain

$$S_{N-1} = \epsilon^{N-1}[U_{N-1}(z) + U_{N-2}(z)] \tag{56}$$

where $U_{N-2}(z)$ is the Chebyshev polynomial of the second kind, i.e.,

$$U_m(z) \equiv \frac{(z+\sqrt{z^2-1})^{m+1} - (z-\sqrt{z^2-1})^{m+1}}{2\sqrt{z^2-1}}.$$

Substituting (56) in (53) and using a property of the Chebyshev polynomials we obtain the following equation:

$$(z+1)[U_{N-1}(z) + U_{N-2}(z)] = 0 \tag{57}$$

which is equivalent to (53).

Equation (57) has a root $z=-1$, hence $q_1 = 0$; i.e.,

$$\lambda^4 + [1+\gamma+\alpha(a-1)]\lambda^3 + [\alpha a+\alpha(a+1)\gamma+\gamma+\beta]\lambda^2 + \alpha[a\gamma+(1+a)\beta]\lambda = 0. \tag{58}$$

To find the values of the other roots we introduce

$$v = z + \sqrt{z^2-1}. \tag{59}$$

$$Q = \begin{vmatrix} \sigma-\lambda & \alpha & 0 & 0 & 0 & 0 & 0 & 0 \\ 1 & -1-\lambda & 1 & 0 & 0 & 0 & 0 & 0 \\ 0 & -\beta & -\gamma-\lambda & 0 & 0 & 0 & 0 & 0 \\ 0 & d & 0 & -\lambda & 0 & -d & 0 & 0 \\ 0 & 0 & 0 & 0 & \sigma-\lambda & \alpha & 0 & 0 \\ 0 & 0 & 0 & 1 & 1 & -1-\lambda & 1 & -1 \\ 0 & 0 & 0 & 0 & 0 & -\beta & -\gamma-\lambda & 0 \\ 0 & 0 & 0 & 0 & 0 & d & 0 & -\lambda \end{vmatrix} \quad \cdots \quad \begin{vmatrix} 0 & 0 & 0 & 0 \\ 0 & 0 & 0 & 0 \\ 0 & 0 & 0 & 0 \\ 0 & 0 & 0 & 0 \\ & & \vdots & \\ \sigma-\lambda & \alpha & 0 & 0 \\ 1 & -1-\lambda & 1 & -1 \\ 0 & -\beta & -\gamma-\lambda & 0 \\ 0 & d & 0 & -\lambda \end{vmatrix}$$

$$\begin{vmatrix} 0 & 0 & 0 & 0 \\ 0 & 0 & 0 & 0 \\ 0 & 0 & 0 & 0 \\ 0 & 0 & 0 & 0 \\ & & \vdots & \\ 0 & 0 & 0 & 0 \\ 0 & 0 & 0 & 0 \\ 0 & 0 & 0 & 0 \\ 0 & 0 & 0 & 0 \end{vmatrix} \quad \ddots \quad \begin{vmatrix} \sigma-\lambda & \alpha & 0 & 0 & 0 & 0 & 0 & 0 \\ 1 & -1-\lambda & 1 & -1 & 0 & 0 & 0 & 0 \\ 0 & -\beta & -\gamma-\lambda & 0 & 0 & 0 & 0 & 0 \\ 0 & d & 0 & -\lambda & 0 & -d & 0 & 0 \\ 0 & 0 & 0 & 0 & \sigma-\lambda & \alpha & 0 & 0 \\ 0 & 0 & 0 & 1 & 1 & -1-\lambda & 1 & 0 \\ 0 & 0 & 0 & 0 & 0 & -\beta & -\gamma-\lambda & 0 \\ 0 & 0 & 0 & 0 & 0 & 0 & 0 & -\lambda \end{vmatrix}$$

Substituting (59) into (57) we obtain

$$(v)^{2N-1} = 1. \tag{60}$$

It follows from (60) and (59) that the other roots of equation (57) are

$$z = z_s,\ z_s \equiv \cos\frac{2\pi s}{2N-1}$$
$$s = 0, 1, \cdots, N-2. \tag{61}$$

These roots provide the equation $q_1 = 2\epsilon(1+z_s)$ which is equivalent to

$$\begin{gathered}\lambda^4 + [1+\gamma+\alpha(a+1)]\lambda^3 + \\ [\alpha a + \alpha(a+1)\gamma + \gamma + \beta + 2d(1+z_s)]\lambda^2 \\ + [\alpha a\gamma + 2d(\gamma+\alpha(a+1))(1+z_s) + \\ \alpha(1+a)\beta]\lambda + 2d\alpha(1+a)\gamma(1+z_s) = 0 \\ s = 0, 1, 2, \cdots, N-2.\end{gathered} \tag{62}$$

Therefore, the Lyapunov characteristic eigenvalues associated with the stationary homogeneous state are determined by (58) and (62). It follows from (58) that the set of these eigenvalues contains a root which has a positive value. Hence, any homogeneous stationary state of the array is unstable. Notice that in the set of the eigenvalues there is one zero root associated with the existence in the system (2), (45) of a one-parameter family of stationary states.

ACKNOWLEDGMENT

The authors are grateful to V. S. Afraimovich and M. I. Rabinovich for useful discussions. Part of this research was carried out while V. I. Nekorkin was DGICYT MEC Visiting Professor at the Instituto Pluridisciplinar, Universidad Complutense de Madrid.

$$S_{N-2} = \begin{vmatrix}
\sigma-\lambda & \alpha & 0 & 0 & 0 & 0 & 0 & 0 & & & & 0 & 0 & 0 & 0 \\
1 & -1-\lambda & 1 & -1 & 0 & 0 & 0 & 0 & & \cdots & & 0 & 0 & 0 & 0 \\
0 & -\beta & -\gamma-\lambda & 0 & 0 & 0 & 0 & 0 & & & & 0 & 0 & 0 & 0 \\
0 & d & 0 & -\lambda & 0 & -d & 0 & 0 & & & & 0 & 0 & 0 & 0 \\
0 & 0 & 0 & 0 & & & & & & & & & \vdots & & \\
0 & 0 & 0 & 1 & & & & & & & & & & & \\
0 & 0 & 0 & 0 & & & & & & & & & & & \\
0 & 0 & 0 & 0 & & & & & & & & & & & \\
 & & & & & & & \ddots & & & & & & & \\
 & & \vdots & & & & & & & & & 0 & 0 & 0 & 0 \\
 & & & & & & & & & & & 0 & 0 & 0 & 0 \\
 & & & & & & & & & & & 0 & 0 & 0 & 0 \\
 & & & & & & & & & & & 0 & -d & 0 & 0 \\
0 & 0 & 0 & 0 & & & & & 0 & 0 & 0 & 0 & \sigma-\lambda & \alpha & 0 & 0 \\
0 & 0 & 0 & 0 & & & & & 0 & 0 & 0 & 1 & 1 & -1-\lambda & 1 & -1 \\
0 & 0 & 0 & 0 & & & & & 0 & 0 & 0 & 0 & 0 & -\beta & -\gamma-\lambda & 0 \\
0 & 0 & 0 & 0 & & & \cdots & & 0 & 0 & 0 & 0 & 0 & d & 0 & -\lambda
\end{vmatrix}$$

and

$$C_{N-2} = \begin{vmatrix}
\sigma-\lambda & \alpha & 0 & 0 & 0 & 0 & 0 & 0 & & & & & & 0 & 0 & 0 & 0 \\
1 & -1-\lambda & 1 & -1 & 0 & 0 & 0 & 0 & & \cdots & & & \cdots & 0 & 0 & 0 & 0 \\
0 & -\beta & -\gamma-\lambda & 0 & 0 & 0 & 0 & 0 & & & & & & 0 & 0 & 0 & 0 \\
0 & d & 0 & -\lambda & 0 & -d & 0 & 0 & & & & & & 0 & 0 & 0 & 0 \\
0 & 0 & 0 & 0 & \ddots & & & & & & & & & & \vdots & & \\
0 & 0 & 0 & 1 & & & & & & & & & & & & & \\
0 & 0 & 0 & 0 & & & & & & & & & & & & & \\
0 & 0 & 0 & 0 & & & & & & & & & & & & & \\
 & & & & & & & \ddots & & & & & & & & & \\
 & & \vdots & & & & & & \sigma-\lambda & \alpha & 0 & 0 & 0 & 0 & 0 & 0 \\
 & & & & & & & & 1 & -1-\lambda & 1 & -1 & 0 & 0 & 0 & 0 \\
 & & & & & & & & 0 & -\beta & -\gamma-\lambda & 0 & 0 & 0 & 0 & 0 \\
 & & & & & & & & 0 & d & 0 & -\lambda & 0 & -d & 0 & 0 \\
0 & 0 & 0 & 0 & & & & & 0 & 0 & 0 & 0 & \sigma-\lambda & \alpha & 0 & 0 \\
0 & 0 & 0 & 0 & & & & & 0 & 0 & 0 & 1 & 1 & -1-\lambda & 1 & 0 \\
0 & 0 & 0 & 0 & & & & & 0 & 0 & 0 & 0 & 0 & -\beta & -\gamma-\lambda & 0 \\
0 & 0 & 0 & 0 & & & \cdots & & 0 & 0 & 0 & 0 & 0 & d & 0 & -d
\end{vmatrix}$$

REFERENCES

[1] S. H. Strogatz and R. E. Mirollo, "Splay states in globally coupled Josephson arrays: Analytical prediction on Floquet multipliers," *Phys. Rev. E*, vol. 47, pp. 220–227, 1993.

[2] Y. Kuramoto, *Chemical Oscillators, Waves, and Turbulence*. New York: Springer-Verlag, 1984.

[3] A. T. Winfree, *The Geometry of Biological Time*. Berlin: Springer, 1990.

[4] G. N. Borisyuk, R. M. Borisyuk, Ya. B. Kazanovich, T. B. Lusyanina, T. S. Turova, and G. S. Cymbalyuk, "Oscillatory neural networks. Mathematics and applications," *Mathematical Modeling*, vol. 3, no. 12, pp. 65–77, 1992 (in Russian).

[5] V. S. Afraimovich, V. I. Nekorkin, G. V. Osipov, and V. D. Shalfeev, *Stability, Structures and Chaos in Nonlinear Synchronization Networks*, Singapore: World Scientific, 1995.

[6] A.-D. Defontaines, Y. Pomeau, and B. Rostand "Chain of coupled bistable oscillators: A model," *Physica D*, vol. 46, pp. 201–216, 1990.

[7] N. F. Rulkov, A. R. Volkovskii, A. Rodriguez-Lozano, E. Del Rio, and M. G. Velarde, "Synchronous chaotic behavior of a response oscillator with chaotic driving," *Chaos, Solitons & Fractals*, vol. 4, no. 1, pp. 201–211, 1994.

[8] V. I. Nekorkin and V. A. Makarov, "Spatial chaoes in a chain of coupled bistable oscillators," *Phys. Rev. Letters*, vol. 74, pp. 4819–4822, 1995.

[9] V. I. Nekorkin, "Traveling pulses in a two-component active medium with diffusion," *Izvestiya VUZ'ov, Radiofizika*, vol. 1, pp. 41–52, 1988 (in Russian).

[10] V. I. Nekorkin and M. G. Velarde, "Solitary wave, soliton bound states and chaos in a dissipative Korteweg-de Vries equation," *Int. J. Bifurc. and Chaos*, vol. 4, pp. 1135–1146, 1994.

[11] M. G. Velarde, V. I. Nekorkin, and A. G. Maksimov, "Further results on the evolution of solitary waves and their bound states of a dissipative Korteweg-de Vries equation," *Int. J. Bifurc. and Chaos*, vol. 5, pp. 831–839, 1995.

[12] V. Pérez-Muñuzuri, V. Pérez-Villar, and L. O. Chua, "Travelling wave front and its failure in one-dimensional array of Chua's circuits," *J. Circuits, Syst. Comput.* vol. 3, pp. 215–229, 1993.

[13] V. Pérez-Muñuzuri, M. Gómes-Gesteira, V. Pérez-Villar, and L. O. Chua, "Travelling propagation in 1-D fluctuating medium," *Int. J. Bifurc. and Chaos*, vol. 3, pp. 211–215, 1993.

[14] V. I. Nekorkin and L. O. Chua, "Spatial disorder and wave fronts in a chain of coupled Chua's circuits," *Int. J. Bifurc. and Chaos*, vol. 3, pp. 1282–1292, 1993.

[15] A. Pérez-Muñuzuri, V. Pérez-Muñuzuri, V. Pérez-Villar, and L. O. Chua, "Spiral waves on a 2-D array of nonlinear circuits," *IEEE Trans. Circuits Syst.*, vol. 40, no. 11, pp. 872–877, 1993.

[16] A. S. Pikovsky and M. I. Rabinovich, "On a strange attractors in physics," in *Nonlinear Waves*, A. V. Gaponov-Grekhov, Ed. Moscow: Nauka, 1979 (in Russian), pp. 176–192.

[17] L. O. Chua, "Global unfolding of Chua's circuits," *IEICE Trans. Fundamental Electron., Commun., Comput. Sci.*, vol. 76–CA, pp. 704–734, 1993.

[18] L. O. Chua, M. Komuro, and T. Matsumoto, "The double scroll family," parts 1 and 2, *IEEE Trans. Circuit Syst.*, vol. CA–33, pp. 1072–1118, 1986.

[19] E. F. Mishenko and N. Rogov, *Differential Equations with the Small Parameter with Highest Derivative and Relaxation Oscillation*. Moscow: Nauka, 1975 (in Russian).

[20] L. P. Shil'nikov, "A contribution to the problem of the structure of an extended neighborhood of a rough equilibrium state of saddle-focus type," *Math. USSR Sb.*, vol. 10, pp. 91–102, 1970.

[21] A. R. Volkovskii and N. F. Rulkov, "Use of one-dimensional mapping for an experimental study of the stochastic dynamics of an oscillator," *Sov. Tech. Phys. Lett.*, vol. 14, pp. 656–658, 1988.

[22] N. F. Rulkov and A. R. Volkovskii, "Experimental analysis of 1-D map from Chua's circuit," in *Chua's Circuit: A Paradigm for Chaos*, R. N. Madan, Ed. Singapore: World Scientific, 1993, pp. 580–590.

[23] C. W. Wu and N. F. Rulkov, "Studying chaos via 1-D Maps—A tutorial," *IEEE Trans. Circuits Syst.—I*, vol. 40, pp. 707–721, 1993.

[24] M. P. Kennedy, "Robust op amp realization of Chua's circuit," *Frequenz*, vol. 46, no. 3–4, pp. 66–80, 1992.

[25] P. Deregel, "Chua's oscillator: A zoo of attractors," *J. Circuits Syst. Comput.*, vol. 3, pp. 309–359, 1993.

[26] R. N. Madan, *Chua's Circuit: A Paradigm for Chaos*, R. N. Madan, Ed. Singapore: World Scientific, 1993.

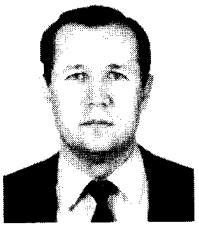

Vladimir I. Nekorkin was born in Ukraine on August 15, 1948. He graduated from the Radio Physics Department of the Nizhny Novgorod State University (NNSU), Russia, in 1971. He received the Ph.D degree in 1981 from NNSU and Degree of Doctor of Science in 1992 from Saratov State University, both in physics and mathemetics.

In 1971, he joined the Institute for Applied Mathematics, Nizhny Novgorod as a Researcher. From 1983 to 1986, he held a position of an assistant professor at the Politechnical Institute, Nizhny Novgorod. In 1986, he joined the Radio Physics Department of the NNSU as an associated professor and became a full professor in 1992. His present reseach interests are in the areas of bifurcation theory and spatio-temporal chaos, pattern formation. He is the author of numerous papers in these areas.

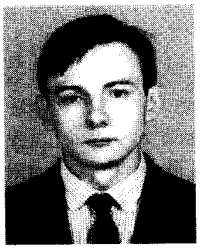

Victor B. Kazantsev was born in Russia on May 9, 1973. He received the M.S. degree in radiophysics from the University of Nizhny Novgorod, Russia, in 1995. His present reseach interests include nonlinear dynamics.

Nikolai F. Rulkov was born in Russia. He received the M.S. degree in 1983 and the Ph.D. degree in 1991, both in physics and mathematics, from the University of Nizhny Novgorod, Russia.

He taught Theory of Nonlinear Oscillations at the Radio Physics Department of the University of Nizhny Novgorod, Russia, from 1987 to 1993. In January 1991, July-September 1991, and July-October 1992, he was with the Facultad de Ciencias, U.N.E.D., Madrid, Spain, as a Visiting Scientist. From February to June 1993, he was on leave at the Department of Electrical Engineering and Computer Sciences, University of California, Berkeley. From June 1993, he is with the Institute for Nonlinear Science, University of California, San Diego. In September 1994, he was on leave at Instituto Pluridisciplinar, Universidad Complutense, Madrid, Spain, as a Visiting Scientist. His research interest are in the areas of nonlinear dynamics, theory of syncronization, and applications of chaotic oscillations in physics and engineering.

Manuel G. Velarde was born on September 7, 1941, in Almeria, Spain. A graduate in physics from the University of Madrid Complutense, he received the Ph.D. degree at the same university in 1968 as well as at the Free University of Brussels in 1970. He also received an Honorary Doctorate in 1994 from the University of Aix-Marseille in France.

Dr. Velarde is currently a Full Professor at the University of Madrid Complutense, where he is the cofounder of its Research Institute Pluridisciplinar. He has held positions at several other universities in France, the UK, Norway, China, and the USA. He has also been a consultant to the Los Alamos Laboratory in New Mexico. The author of numerous research and lay articles, his present interests focus on fluid physics (instabilities, patterns, waves) and nonlinear phenomena at large.

Leon O. Chua (S'60–M'62–SM'70–F'74), for a photograph and biography, see this issue, p. 558.